Summer 8-18-2023

Muscle Defects Lead to Skeletal Deformities in a Zebrafish Model of Distal Arthrogryposis

Emily A. Tomak
University of Maine, emily.tomak@maine.edu

MUSCLE DEFECTS LEAD TO SKELETAL DEFORMITIES IN A ZEBRAFISH MODEL OF DISTAL ARTHROGRYPOSIS

By

Emily Tomak

B.S. The University of Maine, 2021

A THESIS

Submitted in Partial Fulfillment of the

Requirements for the Degree of

Master of Science

(In Biological Sciences)

The Graduate School

The University of Maine

August 2023

Advisory Committee:

Dr. Jared Talbot, Assistant Professor of Biological Sciences, Advisor

Dr. Clarissa Henry, Professor of Biological Sciences

Dr. Joshua Kelley, Assistant Professor of Biochemistry

MUSCLE DEFECTS LEAD TO SKELETAL DEFORMITIES IN A ZEBRAFISH MODEL OF DISTAL ARTHROGRYPOSIS

By Emily Tomak

Thesis Advisor: Dr. Jared Talbot

An Abstract of the Thesis Presented
in Partial Fulfillment of the Requirements for the
Degree of Master of Science
(In Biological Sciences)
August 2023

Distal Arthrogryposis Type 1 (DA1) involves mild muscle weakness and limb skeletal abnormalities thought to be caused by paralysis in utero. Why the limbs are particularly affected in DA1 and the degree of paralysis that leads to these skeletal deformities *in utero* remains unclear. Several muscle genes are known to cause DA1, including MYLPF (myosin light chain phosphorylatable), which encodes a myosin light chain protein that binds close to the force-generating head of myosin heavy chains. The zebrafish *mylpfa*$^{-/-}$ mutant displays a phenotype consistent with DA1, including impaired myosin activity, reduced muscle force overall, and complete fin paralysis. I began my work by analyzing myofibril structure in the *mylpfa*$^{-/-}$ mutant, as well as the *mylpfa*$^{-/-}$*; mylpfb*$^{-/-}$ double mutant which had not been previously characterized carefully. We developed new quantitative techniques to analyze sarcomere formation in high-resolution images, tested the role of Mylpf in sarcomere assembly with statistical rigor, and investigated how these defects impact pectoral fin development. The quantitative suite we developed extends prior image analysis methods by determining the degree to which proteins localize to sarcomere-length repeats within images selected regions of interest from an image are sarcomeric in high-resolution images. To independently verify the

technique, we examined wild-type sarcomere formation and growth from 24-72 hours post fertilization (hpf) and identify unique phases of muscle maturation in this time frame. Then, we applied the method to the *mylpfa*/*mylpfb* datasets, showing quantitatively that sarcomeres are entirely unaffected by *mylpfb* mutation, are partially organized in the *mylpfa*$^{-/-}$ mutant, and are consistently absent when both genes are mutated (*mylpfa; mylpfb* double mutants). Analysis of the pectoral fin region showed that sarcomere defects in the *mylpfa* mutant are nearly as severe as in the *mylpfa*$^{-/-}$*; mylpfb*$^{-/-}$ double mutant. Consistent with the model that DA arises by limb paralysis and the observations that fins are completely paralyzed and lack sarcomeres in the *mylpfa*$^{-/-}$ mutant, I find that the pectoral fin cartilage size is reduced by 25% in the *mylpfa*$^{-/-}$ mutant, a defect that I confirmed using two alleles; this degree of the defect was also consistent across multiple stages of development. Consistent with the observation that both the *mylpfa*$^{-/-}$ mutant and the *mylpfa*$^{-/-}$*; mylpfb*$^{-/-}$ double mutants have complete fin paralysis, I similarly find a 25% reduction in the double mutant. Preliminary analysis of a *Δsix1a;4a*$^{-/-}$*;Δsix1b;4b*$^{-/-}$ mutant completely lacking muscle in the fin shows a more severe fin cartilage defect. These findings suggest that Mylpf gene function is required for sarcomeric protein organization to promote normal fast-twitch muscle and cartilage development.

ACKNOWLEDGEMENTS

Talbot Lab, Summer 2023

Thank you to the entirety of the Talbot lab, but especially to Dr. Jared Talbot, Teresa Easterbrooks, and Tayo Adekeye. To Dr. Talbot for his mentorship and patience. You have taught me so much about science and myself, and I am truly grateful for this experience. Also, thank you to Dr. Talbot for providing the illustrations used in Figures 1, 2, and 6- your Adobe Illustrator and Photoshop expertise is unparalleled. To Teresa for the lunch and work dates, and to Tayo for always being willing to lend a helping hand. Thank you to the 'lab mascot,' my lovely pup Winniford, who worked so hard by my side. Finally, thank you to my family, friends, and my loves, Win and William, who loved and supported me every day of this journey.

The monoclonal antibody, A4.1025, developed by Blau, H.M., was obtained from the Developmental Studies Hybridoma Bank, created by the NICHD of the NIH and maintained at The University of Iowa, Department of Biology, Iowa City, IA 52242.

TABLE OF CONTENTS

LIST OF FIGURES

CHAPTER 1

INTRODUCTION

Arthrogryposis, the term for multiple congenital contractures, affects approximately 1 in 3000 live births (Bamshad, Van Heest, & Pleasure, 2009; Whittle, Johnson, Dobbs, & Gurnett, 2021). Distal arthrogryposis type 1 (DA1), a subset of the arthrogryposes, is a rare genetic disorder characterized by congenital skeletal contractures in the hands and feet and muscle weakness caused by impaired movement in utero (Bamshad et al., 2009). The disease's molecular mechanisms remain poorly understood, and the prevalence of Distal arthrogryposis Type 1 (DA1) is unknown. DA1 is most commonly caused by gene mutations that encode sarcomeric components of muscle fibers, including MYLPF, which encodes a myosin light chain protein that binds close to the force-generating head of myosin heavy chains (Chong et al., 2020). Understanding the molecular mechanisms of MYLPF and its regulation may provide new insights into the pathogenesis of skeletal muscle disorders and potential therapeutic strategies.

The muscle's fundamental contractile unit is the sarcomere, composed of highly organized intercalating F-actin-rich thin filaments and myosin-rich thick filaments (Sanger, Wang, Fan, White, & Sanger, 2010). The sarcomere is a highly organized structure, with specific regions such as the A-band comprised of both actin and myosin filaments, the I-band where the actin filaments are located, the H-zone with only myosin filaments, and the M-line that marks the center of the sarcomere (Krans, Jacob L., 2010; Rui, Bai, & Perrimon, 2010; Z. Wang et al., 2021). The F-actin laden thin filaments are anchored to the Z-disks at either end of the

sarcomere, while thick filaments are near the center of the sarcomere, connected to the thin filaments by cross-bridges. Cross-bridges occur when myosin heads physically bind to the active site of F-actin (Figure 1B). Two types of myosin light chains, the essential and regulatory light chains, structurally support the cross-bridge and bind to the myosin neck to promote contraction (Lowey & Trybus, 2010; Sitbon, Yadav, Kazmierczak, & Cordary, 2020). When ATP activates the myosin heads, they undergo a conformational change and pull the actin filaments toward the center of the sarcomere. This action causes the sarcomere to shorten and the muscle to contract, known as the sliding filament theory (Huxley, 2000; Krans, Jacob L., 2010). Sarcomeres connect end-to-end to form myofibrils, giving myofibrils a striated appearance that is detectable via light microscopy (Rui et al., 2010; Sanger et al., 2010). Each muscle cell, called a myofiber, is syncytial and contains several myofibrils growing from the periphery. Myofibrils parallel one another across many myofibers so force can be produced in a single direction. This is the case for somitic muscles, which are a focus of this study. Zebrafish somites contain both fast and slow-twitch muscle, with fast-twitch muscle composing the inner layers of the somite and slow-twitch muscle the outermost layer (Figure 1A). The superficial slow-twitch fibers are aligned parallel to the zebrafish body axis, and the fast-twitch fibers are aligned at a 45-degree angle pointing to the center of the dorsal-ventral axis, called the horizontal myoseptum.

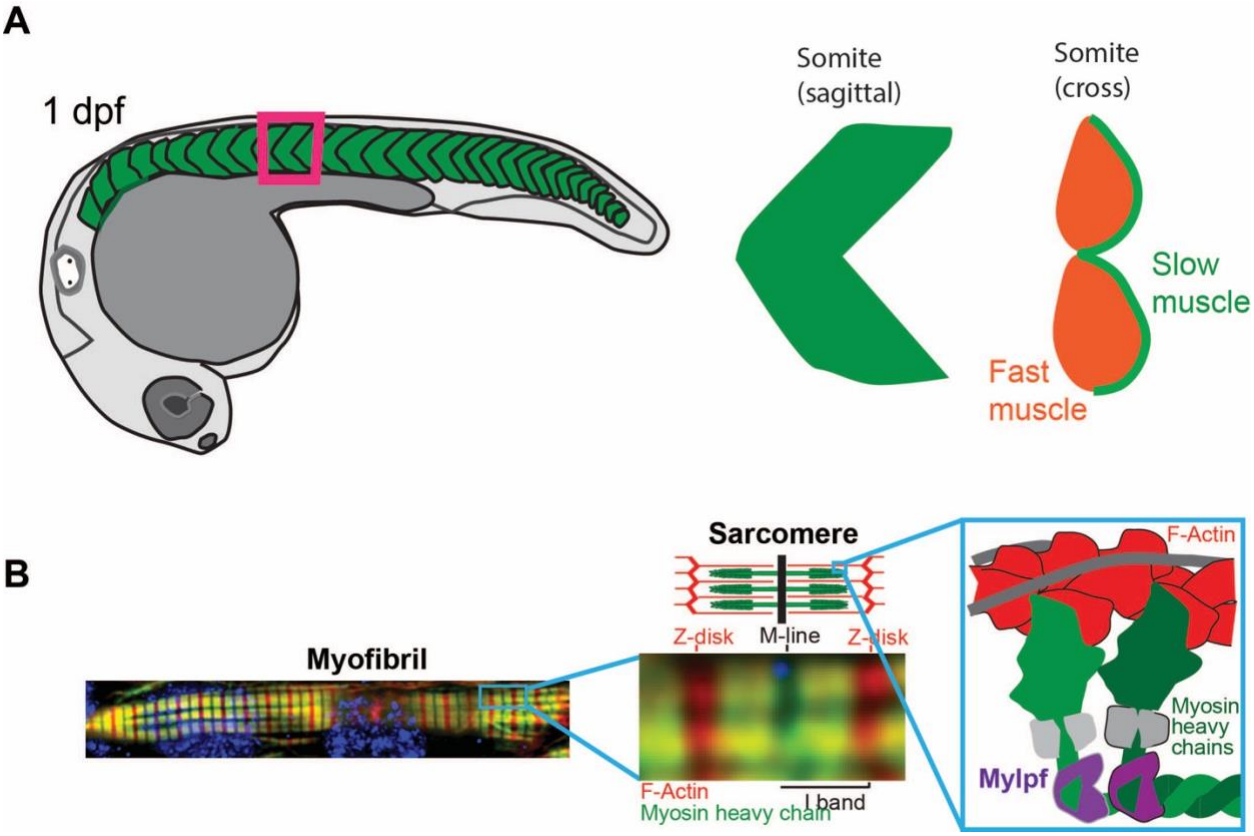

Figure 1. Orientation to Somite Muscle Structure in a Zebrafish Embryo**. (A)** demonstrates somite organization of a 1-day post-fertilization (dpf) zebrafish embryo, with fast-twitch muscle composing the inner layer of the somite and slow-twitch muscle comprising the outermost layer. **(B)** shows a myofibril of a one dpf zebrafish, then simplified to display a labeled sarcomere. F-Actin (red) marks each Z-disk, and Myosin heavy chains are labeled green. The myosin heads then attach to the actin filaments' binding sites to initiate contraction. Two types of myosin light chains, the essential and regulatory light chains, which include Mylpf, structurally support the cross-bridge and bind to the myosin neck to promote contraction.

Many animal models have provided valuable insights into the molecular and cellular mechanisms underlying arthrogryposes. Zebrafish models have been used to investigate the effects of gene mutations that encode myosin light chains on the formation and maintenance of neuromuscular synapses and have been utilized to study the role of DA1-associated genes in

the development and function of the nervous system (Whittle et al., 2021). Zebrafish models have also been used to study the role of essential and regulatory myosin light chains in cardiac function (Chen et al., 2008) and skeletal phenotypic variation (Kimmel et al., 2021). Zebrafish are a unique model for studying musculoskeletal development in vertebrates due to their large clutch size, genetic amenability, rapid growth and development, and transparent embryos (Busse, Galloway, Gray, Harris, & Kwon, 2020; Kimmel, Ballard, Kimmel, Ullmann, & Schilling, 1995; Whittle et al., 2021). In addition to zebrafish, other animal models, such as mice and fruit flies, have also been employed to investigate the molecular mechanisms underlying DA1 and related disorders (Whittle et al., 2021). Knockouts of *Drosophila* RLC or mammalian Mylpf lead to the complete absence of muscle at birth and neonatal lethality due to an inability to breathe (Y. Wang et al., 2007; Whittle et al., 2021). Similarly, in zebrafish, an essential light chain (ELC) gene, *myl7*, was required for normal sarcomere assembly in the heart (Chen et al., 2008).

Although not a member of the Sarcopterygii class (lobe-finned fishes), which is evolutionarily closer to tetrapods, zebrafish provide numerous advantages when studying limb skeletal development (Diogo, Ziermann, Molnar, Siomava, & Abdala, 2018; Mercader, 2007). Zebrafish are beneficial model organisms due to a genome duplication that drove the diversification of teleost lineages, which is increasingly valuable when studying genes with complex functions whose mutations in mammals are lethal (Diogo et al., 2018; Mercader, 2007; Nakamura, Schneider, & Shubin, 2021; Wood & Nakamura, 2018). Understanding the developmental basis of limb evolution can help to understand the etiology of DA1, which is known to be affected by a lack of muscle movement in utero. The development of digits and fin rays in fish share common developmental histories, suggesting that these structures have deep evolutionary

conservation (Nakamura, Gehrke, Lemberg, Szymaszek, & Shubin, 2016; Tulenko & Currie, 2021). Zebrafish (belonging to the teleost class of ray-finned fish, Actinopterygii) have pectoral fin rays instead of a true limb (Grandel & Schulte-Merker, 1998). The development of the paired fins in zebrafish has been compared to the development of the limbs in tetrapods, such as humans. Wrist and digit enhancers in fish are noted to be deeply conserved, indicating that the molecular mechanisms underlying limb development are highly conserved across species (Gehrke et al., 2015). Zebrafish are ray-finned teleost fish that last had a last common ancestor with limb-bearing tetrapods during the Devonian period (Clack, 2009; Nakamura et al., 2016, 2021). Adult fin skeletons are composed of two central tissues: fin rays, which are composed of dermal connective tissue, and endochondral bones. Limbs, including digits, are exclusively comprised of endochondral bones (Diogo et al., 2018; Nakamura et al., 2016, 2021; Schneider & Shubin, 2013). Despite these differences, bony fishes (including teleosts) share genes and developmental regulatory systems used similarly in fin and limb development (Coates, Ruta, & Friedman, 2008; Tulenko & Currie, 2021).

Homologous structures can be identified by the expression of homeodomain (hox) genes, which impart cell identity. Many studies have shown that Hox gene expression is critical in developing limb skeletons and fish fins (Nakamura et al., 2021; Tulenko & Currie, 2021). These studies have revealed that the early steps of paired fin development in zebrafish are like those of tetrapod limb development, suggesting that the genetic mechanisms underlying limb development are evolutionarily conserved (Mercader, 2007). Hox gene expression pattern and function in fin and limb development has provided insight into the evolution of these structures and their functional diversity across different species (Nakamura et al., 2016). During embryonic

development, these genes regulate the placement and growth of structures, such as bones and muscles. In both fins and limbs, Hox genes are expressed in a specific pattern along the anterior-posterior axis, which helps to determine the identity and function of each segment and control the development of limb digits and the number and position of fin rays (Sheth et al., 2012; Wood & Nakamura, 2018).

Mechanical forces play a significant role in musculoskeletal development. Studies in paralyzed chick embryos provided the first indications for muscle-generated forces' involvement in skeletal development (Hamburger & Waugh, 1940; Murray & Drachman, 1969). Building upon earlier studies, Murray and Drachman used neuromuscular blocking agents to induce paralysis of chick embryos *in Ovo*. They noted distortions in cartilaginous and skeletal structures in the head and neck (their primary study region) and atrophy in skeletal muscle and associated connective tissues (Murray & Drachman, 1969). Studies like the one exemplified here revealed that skeletal development is impaired without muscle contraction. These effects of reduced embryonic movement on proper skeletal development were later demonstrated in the chick, the mouse, and the zebrafish, (Osborne, Lamb, Lewthwaite, Dowthwaite, & Pitsillides, 2002; Shwartz, Farkas, Stern, Aszódi, & Zelzer, 2012). It's also been shown in chick embryos that resumption of embryonic movement can help recover joint development following paralysis (Rolfe, Scanlon O'Callaghan, & Murphy, 2021). In zebrafish, immobilization prevented the development of muscular dystrophy (DMD), consistent with observations that inactivity can prolong the life of DMD patients (Li & Arner, 2015), though other work has shown that increased activity in the right contexts can be beneficial (Kilroy et al., 2022). These findings

suggest that movement is essential for normal musculoskeletal development, and its disruption can lead to abnormalities such as arthrogryposis.

Recent exome sequencing identified MYLPF mutations as a cause of DA1 in humans (Chong et al., 2020). Four independent MYLPF variants were discovered in 8 families experiencing distal arthrogryposis. Zebrafish have two MYLPF genes (*mylpfa* and *mylpfb*) due to the teleost genome duplication and the more abundant gene, *mylpfa,* was initially used to investigate the underlying etiology of DA1. Zebrafish *mylpfa* $^{-/-}$ mutants were found to have complete pectoral fin paralysis and an impaired escape response (Chong et al., 2020). Fast skeletal muscle fibers in the *mylpfa* $^{-/-}$ mutants were also deformed, hypothesized to be caused by the degeneration of myofibers completely (Chong et al., 2020). We sought to investigate Mylpf's role in the development and function of skeletal muscles and skeletal development. Prior work by one of Dr. Talbot's undergraduate mentees indicated severe sarcomere defects in the *mylpfa* $^{-/-}$ mutant that becomes even more severe in a small number of *mylpfa* $^{-/-}$; *mylpfb* $^{-/-}$ double mutant animals (Teets, 2018 - Undergraduate Thesis). However, the double mutant dataset was minimal, and it remained unclear how well gene dosage correlated with phenotypic severity and how the limb defects compared to the trunk.

Previous muscle and sarcomere organization quantification methods rely on either Fourier transforms, Haralick texture analysis, or localization analyses (Dunn, Kamocka, & McDonald, 2011; Pasqualini, Sheehy, Agarwal, Aratyn-Schaus, & Parker, 2015; Salick et al., 2020; Stein et al., 2022; Sutcliffe et al., 2018). Sarcomere organization methods utilizing the Fourier transform most commonly apply one-dimensional Fourier transforms to a linear intensity profile across a

large region (Myachina & Lookin, 2020; Pasqualini et al., 2015; Salick et al., 2020). The result of the transform is a wave function that shows the amplitude and phase of each frequency component in the signal. However, there are some scenarios where using a Fourier transform may not be appropriate. When dealing with complex signals with multiple frequencies and varying amplitudes, the Fourier transform may not be effective in capturing the details of the signal (Cerna & Harvey, 2000; Parsons, Boonman, & Obrist, 2000; Salick et al., 2020).

Localization analysis has also been utilized in previous muscle-sarcomere quantification methods (Aoki, Sadoshima, & Izumo, 2000; Bray, Sheehy, & Parker, 2008; Dunn et al., 2011; Lagache et al., 2018; Xu et al., 2012). Colocalization is commonly used in fluorescence microscopy to determine if fluorescently marked molecules associate within the same structure and have been evaluated as a practical guide to understanding protein interactions and cellular processes (Dunn et al., 2011). However, colocalization is not always appropriate for high-resolution image analysis (Dunn et al., 2011).

Sutcliffe's SarcOmere Texture Analysis (SOTA) method utilizes offset distance–angle distributions of Haralick texture features to analyze repeating striations in an entire image, such as a sarcomeres (Stein et al., 2022; Sutcliffe et al., 2018). SOTA recommends a microscope objective of at least 40x, with 63x and 100x being optimal, as the highest magnification gives the best spatial resolution (Stein et al., 2022). Similarly, better results were obtained with SOTA when labeling proteins that are part of the Z-discs or M-lines (e.g., titin, myomesin) than proteins with wider repeat patterns like A-band proteins (actin, troponin). Another limitation of SOTA is that the metric for organization score has a narrow range, from 0 for disorganized to

~0.3 for organized striations, though this sarcomere organization metric could be increased with background subtaction. Likely because of these requirements, we were unable to gain meaningful data from SOTA using our confocal images, and so we sought to develop an independent technique. The quantitative method we developed extends prior image analysis methods by determining the degree to which selected regions of interest from an image are sarcomeric. Our newly developed method does not require whole image analysis or image modification.

In this study, we developed a large dataset, with a triplicate repeat of experiments, containing single and double-mutant animals, developed quantitative techniques for image analysis, tested the role of Mylpf in sarcomere assembly with statistical rigor, and investigated how these defects impact pectoral fin development. By analyzing this dataset, we found that sarcomeres are entirely unaffected by *mylpfb* $^{-/-}$ mutation, are partially organized in the *mylpfa* $^{-/-}$ mutant, and are consistently absent when both genes are mutated (*mylpfa* $^{-/-}$*; mylpfb* $^{-/-}$ double mutants). Analysis of the pectoral fin region showed that sarcomere defects in the *mylpfa* mutant are nearly as severe as in the *mylpfa* $^{-/-}$*; mylpfb* $^{-/-}$ double mutant.

Consistent with the model that DA arises by limb paralysis and the observations that fins are entirely paralyzed and lack sarcomeres in the *mylpfa* $^{-/-}$ mutant, I find that the pectoral fin cartilage size is reduced by 25% in the *mylpfa* $^{-/-}$ mutant, a defect that I confirmed using two alleles; this degree of the defect was also consistent across three stages of development. Consistent with the observation that both the *mylpfa* $^{-/-}$ mutant and the *mylpfa* $^{-/-}$*; mylpfb* $^{-/-}$ double mutants have complete fin paralysis, I similarly find a 25% reduction in the double

mutant. Intriguingly, my preliminary analysis of a mutant completely lacking muscle in the fin (*Δsix1a;4a*$^{-/-}$*;Δsix1b;4b*$^{-/-}$) (Talbot et al., 2019) has an even more severe fin cartilage defect. These findings suggest that physical sarcomere organization defects may underlie the embryonic paralysis and distal limb deformity that characterizes DA1.

CHAPTER 2

A NEW QUANTITATIVE METHOD SHOWS TWO PHASES OF SARCOMERE ASSEMBLY IN THE WILD TYPE ZEBRAFISH

2.1. Developing Quantitative Image Analysis Techniques to Investigate Sarcomere Organization

Standard existing practices like measuring width or sarcomere length are useful but don't directly measure the degree to which structural proteins organize themselves into sarcomeric repeats. Previous unbiased approaches to sarcomere organization quantification methods rely on either Fast-Fourier Transforms, distance–angle comparisons, or localization analyses (Pasqualini et al., 2015; Salick et al., 2020; Sutcliffe et al., 2018). Working with several collaborators, we developed a new technique to determine the degree of sarcomere organization deemed, Sarcomericity. We also built a tool to speed comparisons of myofibril width per fish, instead of per myofibril, allowing for efficient measurement of measurements like myofibril width or sarcomere length. With this tool, the individual specimen is set as the N, so all N are truly biologically independent. This package was developed with additions from Dr. Joshua Kelley, Dr. Joy-El Talbot, Dr. Jared Talbot, and myself. Sarcomericity analysis allows us to determine the fraction of total protein that has the same periodicity as a sarcomere, and can be applied to multiple markers, including common ones like F-Actin. This method uses multiple Range of Interest (ROI) delineations in ImageJ to calculate intensity per ROI for each image channel. Then, peak-to-peak distances per intensity are determined per image, then averaged

to show bootstrap confidence intervals shown via histogram to represent the Fraction of Peaks/micron (μm). The histogram analysis is then used to determine Sarcomericity in MATLAB. The sarcomericity score is achieved by identifying the typical sarcomeric region in bin ranges for each marker, then by dividing the sum of the sarcomeric histogram region by the total, allowing for the Sarcomericity score to be on an intuitive scale from 0 (not sarcomeric) to 1 (entirely sarcomeric). Additionally, I developed scripts to quickly measure myofibril thickness, which gives a rapid proxy for sarcomere development. The methodology for each image analysis step is explained in detail in Chapters 5.6-5.7.

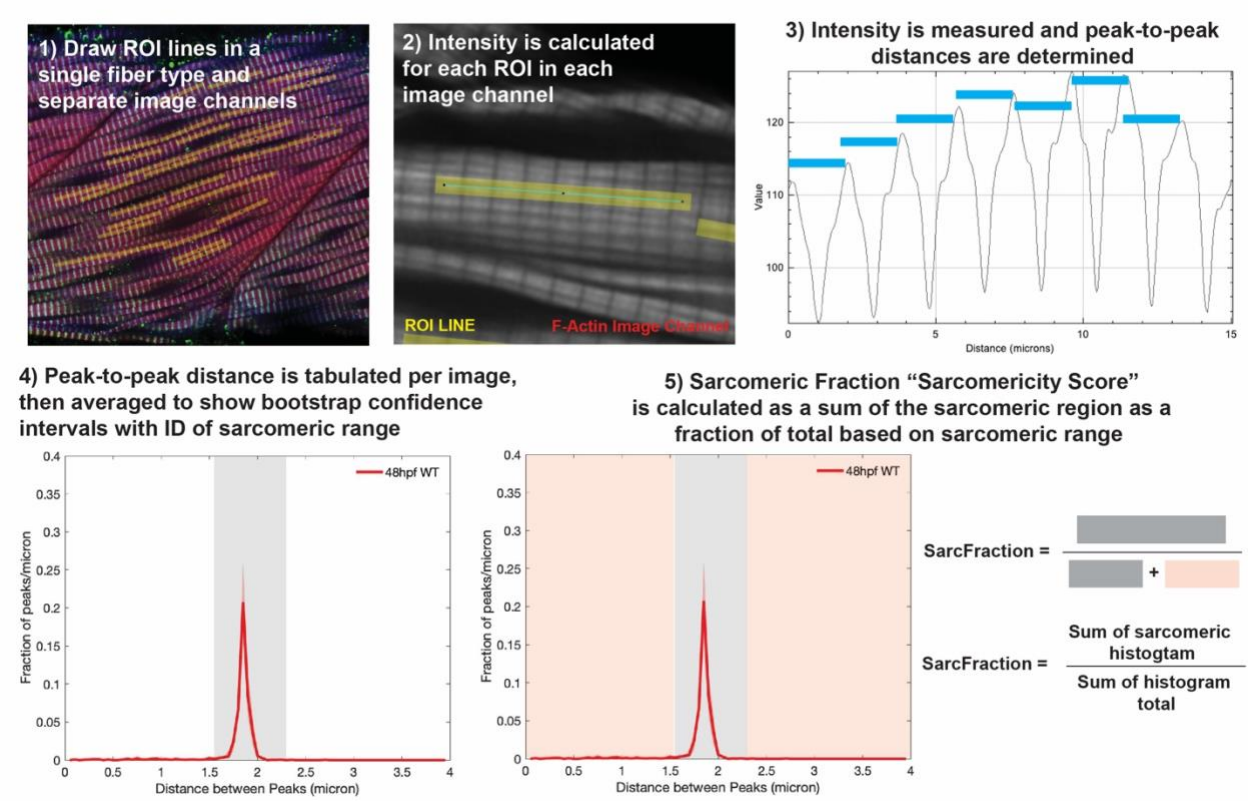

Figure 2. Workflow of Sarcomericity Image Analysis Package. **(1)** demonstrates multiple ROI lines used to quantify sarcomere organization in a single fiber type. **(2)** ROI lines are used to calculate intensity profiles in each image channel. **(3)** Intensity profiles are used to determine peak-to-peak distances per ROI. **(4)** Peak-to-peak distances are calculated per image and image

channel, then averaged across genotypes to show 95% bootstrap confidence intervals with a gray box overlay to identify the sarcomeric length range. **(5)** The "Sarcomericity Score" takes the sum of the area of the sarcomeric region divided by the sum of the total area to score intuitively from 0-1, 0 being the most disorganized to 1 being highly organized.

2.2. Sarcomericity Analysis Identifies Two Phases of Sarcomere Formation: Localization (24-48 hpf) and Growth (48 hpf Onwards)

To demonstrate the ability of our quantification tool to determine differences in sarcomeric structure and organization during normal development, I applied it to Wild-Type fish fixed at three time points (24 hpf, 48 hpf, and 72 hpf) when myofibrils form and undergo radical change. At each stage, we labeled embryos with the Z-disk marker Actinin, the F-Actin marker Phalloidin, and the sarcomere-width marker Titin. This analysis shows that Actinin becomes increasingly localized to the sarcomere between 24 hpf and 48 hpf (Figure 3F, I, L). Myofibril width increases consistently between 24 hpf, 48 hpf, and 72 hpf, demonstrating continuous growth across all three time points in fast-twitch muscle (Figure 3M). However, although myofibril width in fast-twitch muscle continues to increase throughout the whole time period, the sarcomericity fraction reaches its maximum by 48 hpf. This same pattern was found for Actinin, Titin, and F-Actin markers, suggesting that sarcomeric components organize locally in fast-twitch muscle by 48 hpf in zebrafish (Figure 3D-E, J-K). We found similar localization changes in fast-twitch and slow-twitch muscle fibers and similar sarcomere lengths in both fiber types, though the slow-twitch fibers show an early relaxed state of sarcomere length at 24 hpf before sarcomeric maturation in F-Actin and Actinin (Figure 3G, I). Sarcomere lengths were

initially calculated using the programs we developed, then manually verified across all time points. This analysis indicates that most contractile proteins in a cell localize to sarcomeres by 48hpf (Figure 3J-L). After that, newly synthesized contractile proteins can rapidly localize to sarcomeres, driving rapid sarcomere and myofibril growth (Figure 3K). These findings show that the sarcomericity quantitation technique we developed can detect changes in muscle structure through time. By 48 hpf, nearly all F-Actin and MyHC are incorporated into myofibrils, leading to efficient growth. From this point onwards, the myofibers have a set sarcomere length of 1.8 µm. However, initially, the SMC sarcomeres are longer (2.2 µm at 24 hpf) and much of the sarcomeric protein does not localize to sarcomeric repeats. Together these findings point to an initial phase of inefficient myofibril growth (24-48 hpf) followed by rapid integration of sarcomeric protein to the myofibrils (48 hpf onwards).

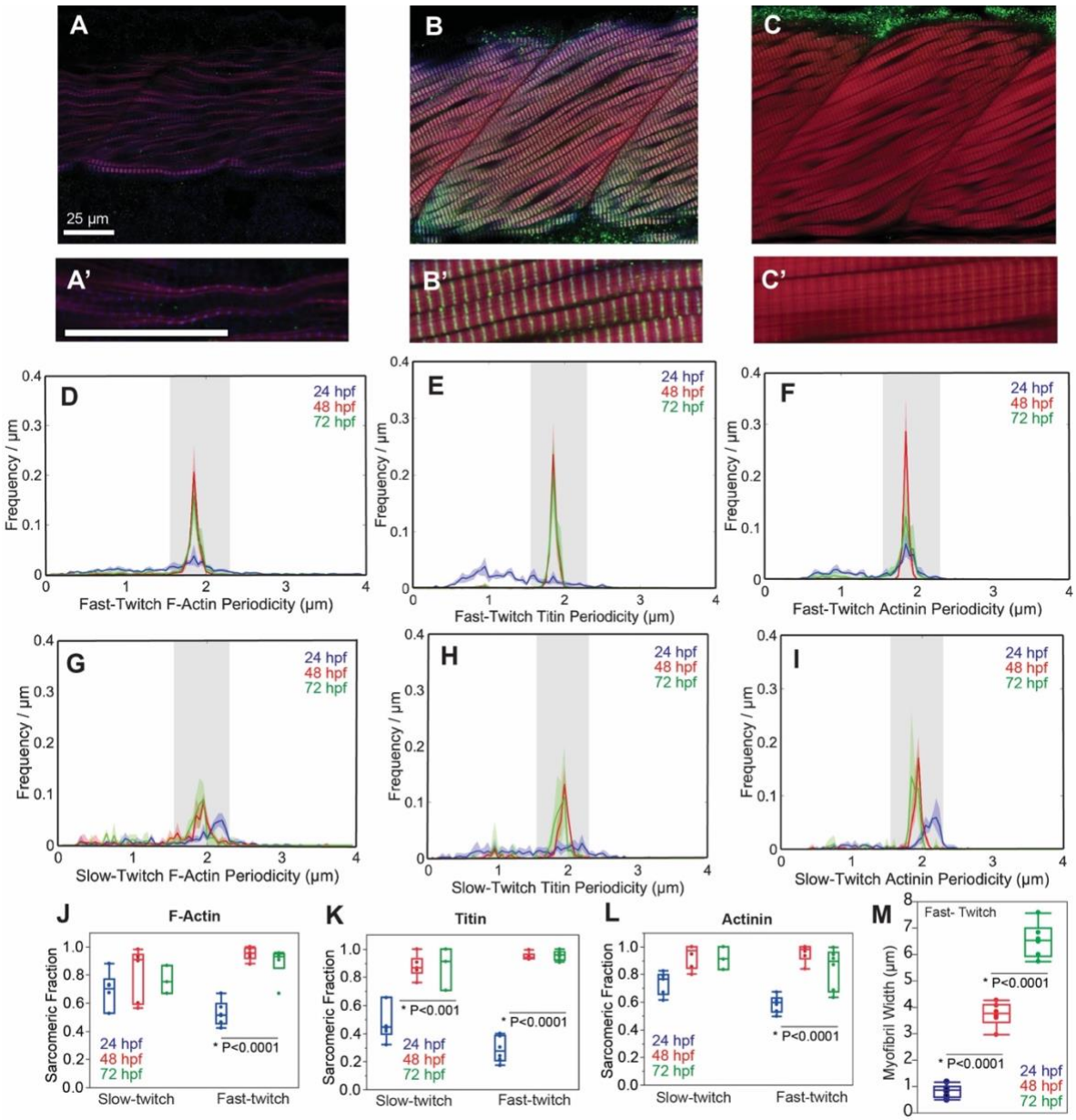

Figure 3. Sarcomeric Proteins Organize by 48hpf in Zebrafish Embryos. **(A-C')** Immunolabel of sarcomere components and myonuclei in 24hpf WT (A), 48hpf WT (B), and 72hpf WT (C). Phalloidin label marks F-actin (red), a Titin antibody (green) marks Titin, and an antibody anti-actinin marks actinin (blue). **(A-C)** show developing fast muscle fibers in 24hpf WT (A), 48hpf WT (B), and 72hpf WT (C). **(A'-C')** Zoomed insets of fast muscle fibers highlight the myofibrillar structure. **(D-I)** Quantification of sarcomere organization, shown as a histogram plot of image periodicity in slow (G-I) and fast-twitch (D-F) muscle. In both fast and slow-twitch muscles, there is a significant increase in sarcomere organization from 24hpf to 48hpf, with no significant change from 48hpf to 72hpf across all markers. Mean lines are shown in a dark color for each time point, and 95% bootstrapped confidence intervals are shown with shading. Gray box overlays indicate the identified sarcomeric length range. **(J-L)** Fraction of the F-Actin, Titin, and

Actinin signals in the sarcomeric length range shows the same trends across all time points in both fast and slow-twitch muscles. **(K)** Myofiber width demonstrates myofibrillar growth in fast-twitch muscle despite organization by 48hpf. Scale bars in A and A' are 25 μm, applicable to their row. Significance thresholds were determined by Tukey-Kramer comparisons after one-way ANOVA.

2.3. New Quantitative Image Analysis Reveals Insights into Sarcomere Development and Organization in WT

To quantify the onset of sarcomeric organization in high-resolution images, we developed an unbiased sarcomere organization quantification method, deemed Sarcomericity. Existing muscle-sarcomere quantification methods were first utilized to quantify our high-resolution images. Colocalization is one of the most common metrics used in fluorescence microscopy, and it can be used to determine if two sarcomeric proteins overlap one another, but doesn't directly test whether they are organized into sarcomeric repeats and also is not useful in single-channel analysis. The SOTA method utilizes offset distance–angle distributions of Haralick texture features to analyze repeating striations in an entire image, such as a sarcomeres (Stein et al., 2022; Sutcliffe et al., 2018). However, SOTA works best when labeling proteins that are part of the Z-discs or M-lines (e.g., titin, myomesin) than with A-band proteins (actin, troponin) (Stein et al., 2022). Our sarcomericity image analysis package was applied to multiple datasets, first to WT zebrafish embryos at various stages to investigate the sarcomeric organization and myofibril development through time and does not require whole image analysis or image modification, and can be applied to multiple proteins throughout the entire sarcomeric repeat.

While analyzing Actin, Titin, and Actinin muscle immunolabel markers, sarcomere organization increased significantly between 24hpf and 48hpf, with no significant increase between 48hpf and 72hpf in both fast and slow-twitch muscle. The Z-disk links titin and actin filaments from opposing sarcomere halves connected by alpha-actinin, making these valuable markers for analyzing sarcomere organization and periodicity through time. Interestingly, analysis of slow-twitch muscle using these same markers and time points mirrors findings in fast-twitch muscle but shows an early relaxed state of sarcomere length at 24hpf before sarcomeric maturation, suggesting a state of lax tension before sarcomeric contractile proteins localize to the cell. Myofibril width analysis showed a significant increase in all time points. This data indicates that sarcomeric contractile proteins localize to sarcomeres by 48hpf and can then rapidly organize newly synthesized sarcomeric contractile proteins resulting in tension necessary to drive myofibril growth (Luis & Schnorrer, 2021; Mao et al., 2022).

CHAPTER 3

SARCOMERES ARE DISARRAYED IN ZEBRAFISH MUTANT FOR THE Mylpf GENES

Unpublished work from Sharon Amacher's lab at The Ohio State University by Dr. Talbot and his mentee Emily Teets indicated severe sarcomere defects in the *mylpfa* $^{-/-}$ mutant (Teets, 2018 - Undergraduate Thesis) that becomes even more severe in a small number of *mylpfa* $^{-/-}$*; mylpfb* $^{-/-}$ double mutant animals. Visual examination of these Mylpf mutants seemed to show a striking gradation of myofibril formation, from "completely normal" (*mylpfb*$^{-/-}$) to "none at all," (*mylpfa*$^{-/-}$*;mylpfb*$^{-/-}$) and we wished to devise a quantitative method that would interpret changes across this whole span.

Preliminary analysis of th*e mylpfa*$^{-/-}$ mutant suggested that this gene had a critical role in myofibril formation. However, prior to my work, the lab had only analyzed 2 double mutant fish using immunolabel at 48 hpf and 3 using TEM at 72 hpf. To begin, I sought to develop a robust dataset of animals to compare the WT, *mylpfa*$^{-/-}$, *mylpfb*$^{-/-}$, and double-mutant genotypes in comparable conditions. Much of my work was focused on high resolution images at the 48 hpf time point with 10 WT, 10 mylpfb$^{-/-}$, 5 doubly heterozygous *mylpfa*$^{+/-}$*;mylpfb*$^{+/-}$,8 *mylpfa*$^{-/-}$, 8 *mylpfa*$^{-/-}$*;mylpfb*$^{+/-}$ (homozygous mutant for *mylpfa*, heterozygous for *mylpfb*), and 11 doubly homozygous *mylpfa* $^{-/-}$*; mylpfb* $^{-/-}$ used for image analysis. For instance, the resolution in WT images is high enough to show black space between thin filaments at the M-line, which is a gap of only 0.15 µm. Measurements of M-line widths across 10 WT images, from multiple imaging days, reveal a gap of 0.147 µm with a standard deviation of 0.029, indicating that our

resolution is sufficient to separate key substructural elements of the sarcomere. At this 48 hpf time point, we exclusively examined somite muscles, because, at that time, other muscle groups like the hypaxial and cranial muscles are only just starting to form.

3.1. Mylpf Gene Function is Essential to Fast-Twitch Muscle Development

Dr. Talbot and I imaged animals from the 48 hpf time point and then applied the Sarcomericity Image Analysis package to these images. Both actin and myosin markers revealed that slow-twitch fibers are spared in the *mylpfa*$^{-/-}$ mutants, versus fast-twitch fibers in *mylpfa*$^{-/-}$ mutants showed a significant decrease in sarcomericity compared to WT. When analyzing Myosin Heavy Chain (MyHC) and Actin markers, fast-twitch fibers in WT and *mylpfb*$^{-/-}$mutants showed no significant decrease in sarcomericity between genotypes, whereas *mylpfa*$^{-/-}$ *and mylpfa*$^{-/-}$*;mylpfb*$^{-/-}$ double mutant fast-twitch fibers all showed significant decreases in sarcomere organization and myofibril width when compared to WT and *mylpfb*$^{-/-}$ mutants (Figure 4I-N). However, there is a small amount of sarcomericity in the double mutant, indicating a partial organization of thin and thick and thin filaments which is also seen in the equally severe mutants *mylpfa*$^{+/-}$*;mylpfb*$^{-/-}$ mutants (Figure 4K, N). Doubly heterozygous *mylpfa*$^{+/-}$*;mylpfb*$^{+/-}$ mutant fish demonstrated a smaller myofibril width when compared to WT and *mylpfb*$^{-/-}$ mutants, corresponding to gene dosage. Slow-twitch fibers showed consistent and normal sarcomericity and myofibril width (Figure 4O) using MyHC (Figure 4K) and Actin (Figure 4N) markers across all genotypes. Double Multiple datasets from multiple days of imaging were merged for grayscale analysis. Across these datasets, no differences were found when analyzed both separately and together. Combined normalized grayscale intensity levels show no change

in F-Actin or MyHC protein levels across genotypes (Figure 4P). These findings further support that Mylpf genes are essential for sarcomere organization in fast-twitch fibers and that Mylpf gene dosage affects sarcomere assembly and organization.

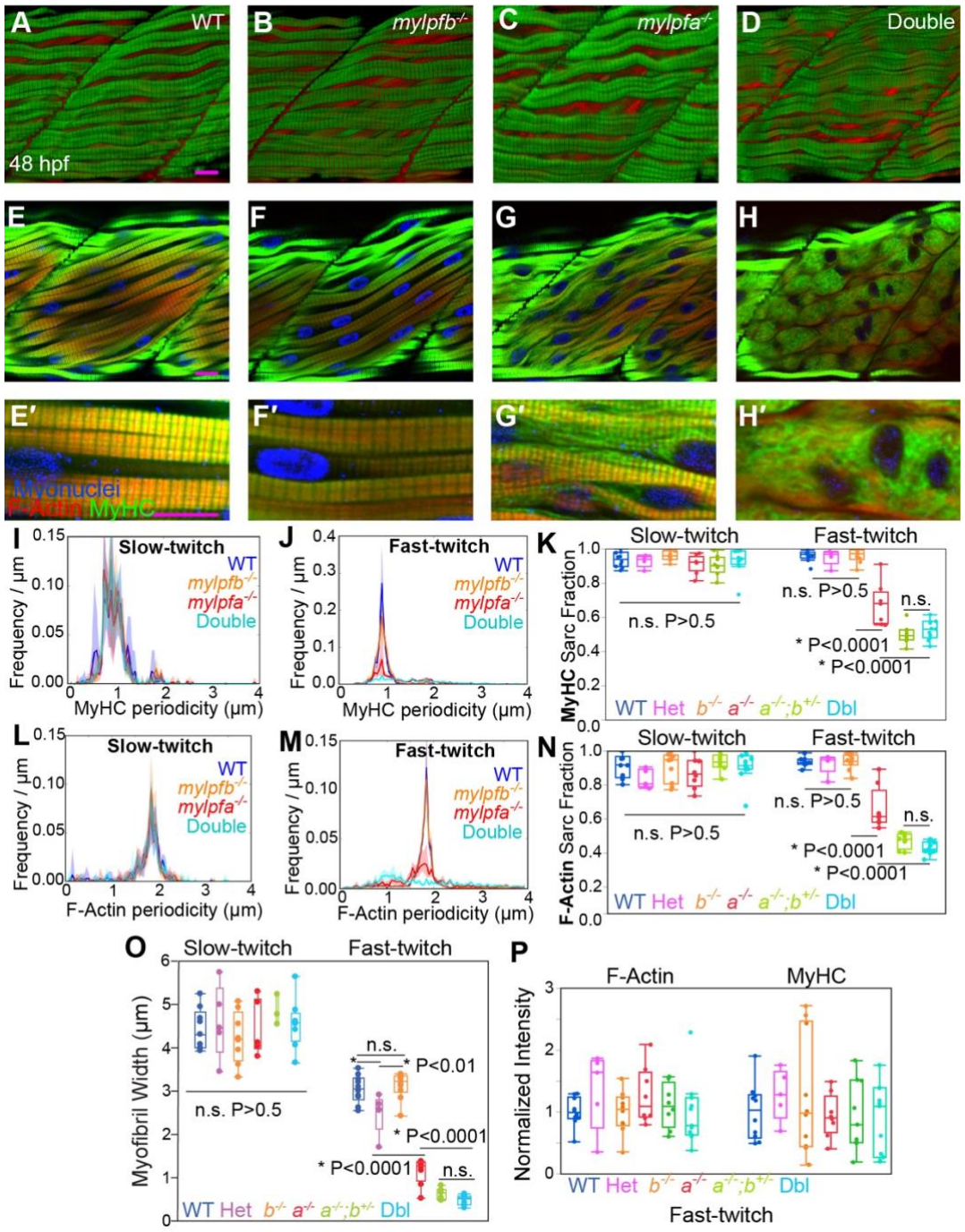

Figure 4. Both Mylpf Genes Contribute to Sarcomere Formation in Fast-Twitch Skeletal Muscle. **(A-H')** Immunolabel of sarcomere components and myonuclei in WT (A), *mylpfb*$^{-/-}$ (B), *mylpfa*$^{-/-}$ (C), and the *mylpfa*$^{-/-}$;*mylpfb*$^{-/-}$ double mutant (D). Phalloidin label marks F-actin (red), antibody A4.1025 (green) marks skeletal muscle MyHC and antibody to Rbfox1l marks myonuclei (blue). **(A-D)** 3D render of the confocal stack shows normal sarcomere organization in slow muscle fibers, which are on the surface of the embryo's muscle, independent of genotype. **(E-H)**

in a deeper slice, the fast muscle fibers can be seen; these appear WT (E) in the *mylpfb*$^{-/-}$ mutant (F) but are overt myofibrillar defects in the *mylpfa*$^{-/-}$ mutant (G), and no myofibrils in the *mylpfa*$^{-/-}$*;mylpfb*$^{-/-}$ double mutant (H). **(E'-H')** Zoomed insets of fast muscle fibers highlight myofibrillar structure (A''-D''). **(I-K)** Quantification of MyHC organization, shown as a histogram plot of image periodicity in slow (I) and fast-twitch (J) muscle and summarized as a fraction sarcomeric (K). **(L, M)** Quantification of actin periodicity supports this gradation of sarcomeric ordering in slow-twitch (I) and fast-twitch (J) fibers. In the WT and *mylpfb*$^{-/-}$ mutant, most of the Actin channel is arrayed with a period of 1.8 µm; however, this peak of image-ordering is reduced in the *mylpfa*$^{-/-}$ mutant and lost in the *mylpfa*$^{-/-}$*;mylpfb*$^{-/-}$ double mutant. For each genotype, mean lines are shown in a dark color, and 95% bootstrapped confidence intervals are shown with shading. **(N)** Fraction of the F-Actin signal in the sarcomeric length range shows the same trends across genotypes. **(O)** Myofibril width further confirms myofibrillar defects in the *mylpfa*$^{-/-}$ mutant and no myofibrils in the *mylpfa*$^{-/-}$*;mylpfb*$^{-/-}$ double mutant. **(P)** Grayscale image analysis demonstrates that although fast twitch muscle is disorganized in the *mylpfa*$^{-/-}$ mutant and lost in the *mylpfa*$^{-/-}$*;mylpfb*$^{-/-}$ double mutant, there is no loss in sarcomeric protein signal. Scale bars in A, A', and A'' are 10 µm, applicable to their row. The scale bar in I is 1 µm, applicable to I-K. Significance thresholds were determined by Tukey-Kramer comparisons after one-way ANOVA.

3.2. A Model for Mylpf Gene Function in Sarcomere Assembly

Prior studies of Mylpf found that fast skeletal muscle fibers in the *mylpfa*$^{-/-}$ mutants were deformed, hypothesized to be caused by the degeneration of myofibers completely (Chong et al., 2020). Similarly, a knockout of *Drosophila* RLC or mammalian Mylpf leads to the complete absence of muscle at birth and neonatal lethality due to an inability to breathe (Y. Wang et al., 2007; Whittle et al., 2021). In utero, mouse has only one fiber type, the 'embryonal fiber type'. We hypothesize that Mylpf is the key RLC in embryonal myofibers, and that it only adopts a fiber-type specific role in mammals postnatally. Our results utilizing Actin and Myosin markers, the key components to sarcomere formation and function, show that fast-twitch muscle form only partially in *mylpfa*$^{-/-}$ mutants and are reduced in the *mylpfa*$^{-/-}$*;mylpfb*$^{-/-}$ double mutant.

We developed a large dataset of single and double-mutant animals, developed quantitative techniques for image analysis, and tested the role of Mylpf in sarcomere assembly and myofibril development with statistical rigor. Visual inspection of the images showed a consistent pattern across genotypes. Consistent with findings that *mylpfa* is expressed exclusively in fast-twitch muscles, we only found defects in fast-twitch muscles, suggesting that the gene is required cell-autonomously. Within this fast fiber type, in all datasets, we could visually observe a reduction of myofibrils and sarcomeres in the *mylpfa*$^{-/-}$ mutant and an apparent reduction of both in the double mutant. Our quantification supports the consistency of these phenotypes in each genotype (Fig 4 I-O). Specifically, we found that fast-twitch sarcomericity is entirely unaffected by *mylpfb*$^{-/-}$ mutation, and sarcomericity is reduced to 60% in the *mylpfa*$^{-/-}$ mutant and reduced to 40% in the *mylpfa*$^{-/-}$*;mylpfb*$^{-/-}$ double mutant, supporting that Mylpf genes are essential for sarcomeric protein organization in fast-twitch fibers. An unpublished Western Blot analysis completed by Sadie Waterman, an undergraduate in the Talbot Lab, found that the *mylpfa*$^{-/-}$ mutants lack around 60% of the total Mylpf protein, coinciding with a similar decrease in sarcomericity (Waterman, 2023 - Capstone Paper). Grayscale values indicate that F-Actin and MyHC proteins remain unchanged across genotypes, supporting that the sarcomere organization defect is primarily a localization defect rather than affecting protein levels. Sadie Waterman tested this idea further using western blot and found no difference in MyHC nor Actinin protein levels (Waterman, 2023 - Capstone Paper). We propose that the remaining sarcomeric fraction in the double mutant can be explained by the formation of thick filaments and I-Z-I bodies (Figure 5- Model). Consistent with this model, we find that myofibril width is reduced in the double mutant, which have only actin pre-myofibrils

along its periphery (Figure 5). Myofibril width analysis of Mylpf mutants revealed a phenotype consistent with Mylpf gene dosage, showing that double heterozygous zebrafish fast-twitch myofibrils were reduced compared to WT and *mylpfb*$^{-/-}$ mutants. The decreased myofibril width of the double heterozygous fish is consistent with Mylpf gene dosage- whose gene dosage is half that of WT.

The absence of sarcomeres and myofibrils in the *mylpfa*$^{-/-}$*;mylpfb*$^{-/-}$ double mutant demonstrates that fast-twitch muscle fibers in these Mylpf mutants do not degenerate but fail to form adequately. Sarcomericity analysis of multiple genotypes identified no significant sarcomere organization differences in WT, double heterozygous, and *mylpfb*$^{-/-}$ mutations but indicated partial sarcomere organization in the *mylpfa*$^{-/-}$ mutant, indicating some genetic compensation from *mylpfb*. Failure of actin and myosin to interdigitate was further confirmed via electron microscopy, where the *mylpfa*$^{-/-}$ mutant muscle under an electron microscope where aggregates of thick and thin filaments were present but only sometimes organized to form I-Z-I bodies. In the double mutant, thick filaments were present and thin filaments were correctly connected via Z- disks, forming I-Z-I bodies or connecting thin filaments and Z-lines. However, the I-Z-I bodies do not overlap with thick filaments. We find a similar pattern in hypaxial muscles when we examined 7 WT, 2 *mylpfa*$^{-/-}$, 2 *mylpfb*$^{-/-}$, and 6 *mylpfa*$^{-/-}$; *mylpfb*$^{-/-}$, double mutants (see Chapter 4.1). These findings suggest that Mylpf gene function is needed for normal interdigitation of myosin with actin into functioning sarcomeres in fast-twitch muscles (Figure 5).

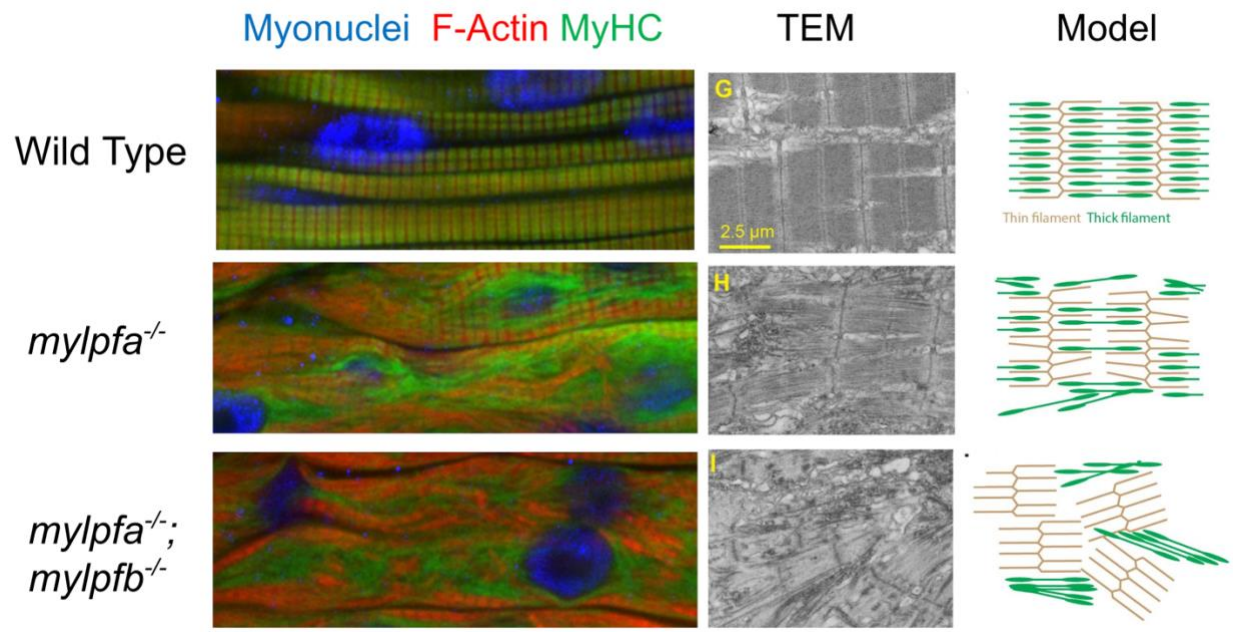

Figure 5. Mylpf Mutant Fish Have Severe Structural Defects**.** Sarcomere assembly and organization are shown in 48hpf WT, *mylpfa*$^{-/-}$, *mylpfa*$^{-/-}$;*mylpfb*$^{-/-}$ zebrafish embryos. The model demonstrates the proposed thin and thick filament interdigitation for each genotype. This model excludes *mylpfb*$^{-/-}$ mutants and other intermediary genotypes, due to a lack of sample size for electron microscopy. Electron microscopy data by Dr. Talbot.

We find that myofibril development is gene-dose dependent, with doubly heterozygous mutants having a decreased myofibril width while maintaining sarcomere organization, strongly implicating that Mylpf is required for myofibril development in fast-twitch fibers. Sarcomeres in Mylpf mutants fail to form adequately, resulting in little muscular tension, which coordinates the assembly of key sarcomeric components to myofibrils that further mature during development (Luis & Schnorrer, 2021; Mao et al., 2022). Our results indicate that the lack of proper sarcomere development could be responsible for the muscle weakness experienced by human patients with DA1.

CHAPTER 4

SARCOMERE ORGANIZATION IS NEEDED FOR NORMAL CARTILAGE FORMATION IN THE ZEBRAFISH PECTORAL FIN

4.1. Understanding Fin Muscle Development in Relation to Cartilage

DA1 affects the joints and muscles of the extremities, causing skeletal deformities primarily in the distal limbs. Individuals with this condition typically have limited mobility in their fingers, wrists, elbows, ankles, and knees, which can result in a characteristic "hooked" appearance of the hands and feet. Other skeletal abnormalities may include curved fingers, overlapping toes, and a fixed bent position of the joints (J. G. Hall, 2014; J. G. Hall & Kiefer, 2016). It's long been known that muscle movement is required for aspects of normal skeletal development and that paralysis often results in skeletal deformities, though different skeletal elements vary in the degree to which they are shaped by movements and when the movements are required (B. K. Hall & Herring, 1990). Because of this connection between muscle-driven movement and skeletal development, and the observation that babies with arthrogryposis often experienced a period of impaired movement, paralysis in utero has long been hypothesized as a cause of arthrogryposes including DA (J. G. Hall, 2014; J. G. Hall & Kiefer, 2016). Consistent with this model, it was recently found that the zebrafish *mylpfa*$^{-/-}$ mutant displays total fin paralysis and detrimental *MYLPF* gene variants are found in some human DA1 patients (Chong et al., 2020).

We sought to understand why Mylpf mutations lead to partial limb skeletal deformities and how this may affect our understanding of DA1 development. We have shown that sarcomere

organization and myofibril development in the zebrafish trunk is impaired in *mylpfa*$^{-/-}$ and *mylpfa*$^{-/-}$*;mylpfb*$^{-/-}$ double mutant fast-twitch fibers and sought to understand how this affects the development of the fin, which is wholly composed of fast-twitch fibers and whose muscle only begins to differentiate at 2 days post fertilization (dpf) with movement beginning at 3 dpf (Figure 6A) (Chong et al., 2020). We zoned in on the zebrafish pectoral fin, specifically the cartilage-composed endochondral plate with overlaying fast-twitch fibers, which is analogous to the human distal limb (Figure 6B) (Gehrke et al., 2015; Mercader, 2007; Nakamura et al., 2016, 2021; Tulenko & Currie, 2021).

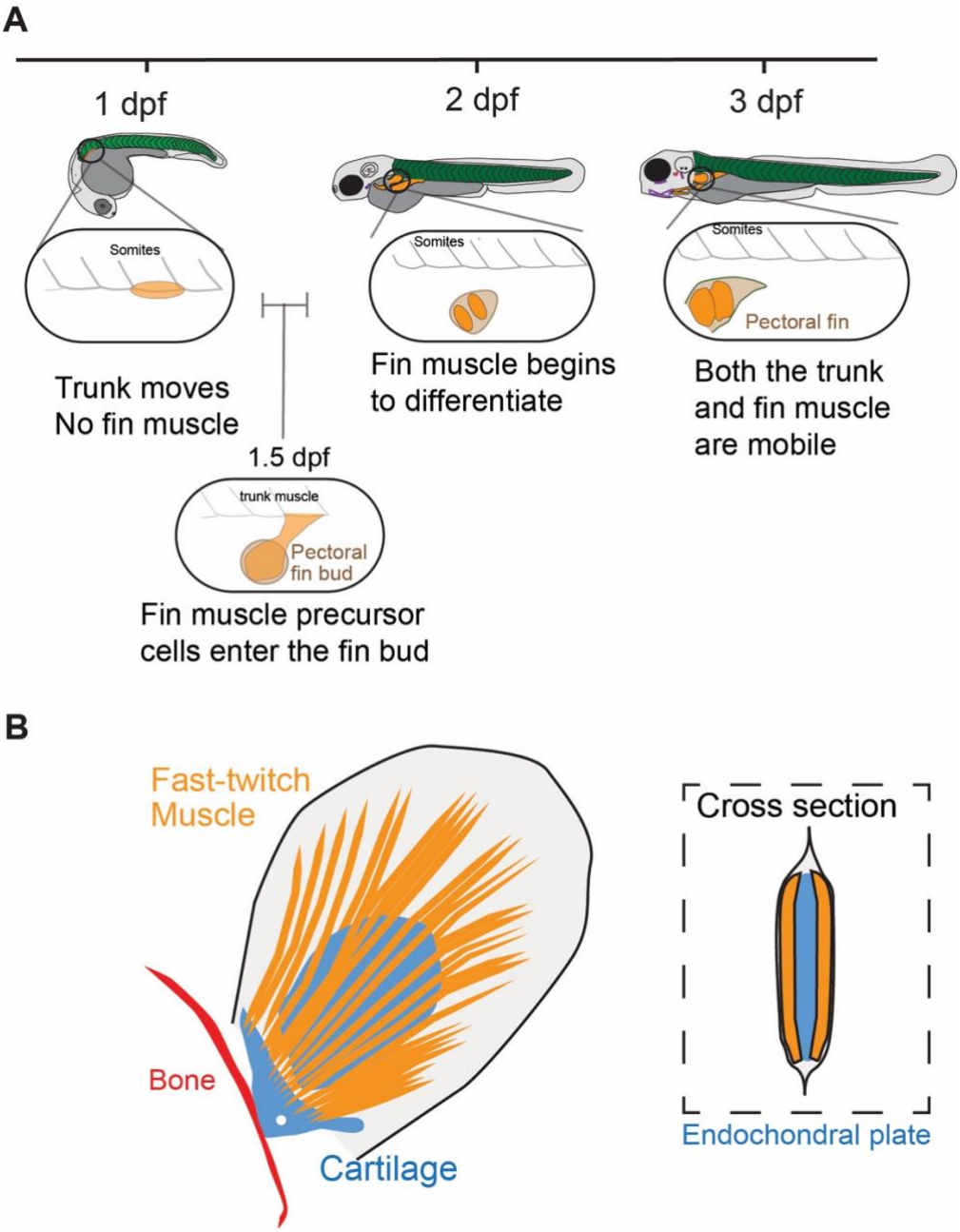

Figure 6. Development and Physiology of the Zebrafish Pectoral Fin. **(A)** demonstrates zebrafish pectoral fin muscle development from 1 dpf to 3 dpf. **(B)** shows the morphology of a zebrafish embryo pectoral fin. Cartilage (blue) makes up the distal fin, and bone (red) comprises the most proximal. The endochondral plate, or most distal cartilage element, is completely encapsulated by fast-twitch muscle fibers which comprise the pectoral fin. Figure by Dr. Talbot.

We chose to study the pectoral fin muscles and posterior hypaxial muscle (PHM) development in 3 dpf zebrafish embryos. The pectoral fin and PHM muscles begin to differentiate at 2 dpf and are fully mobile at 3 dpf (Figure 6A). Immunolabel of sarcomere components in 3 dpf PHM and fin muscle in *mylpfa*$^{-/-}$ and *mylpfa*$^{-/-}$*;mylpfb*$^{-/-}$ double mutants revealed similar myofibril defects as in the trunk, where 3 dpf WT and *mylpfb*$^{-/-}$ mutants remained unaffected (Figure 7 A-D). Preliminary myofibril width analysis demonstrated a reduction in width in both *mylpfa*$^{-/-}$ and *mylpfa*$^{-/-}$*;mylpfb*$^{-/-}$ double mutant when compared to WT and *mylpfb*$^{-/-}$ mutants in both the PHM and fin muscle, closely mirroring findings in the trunk (Figure 7E).

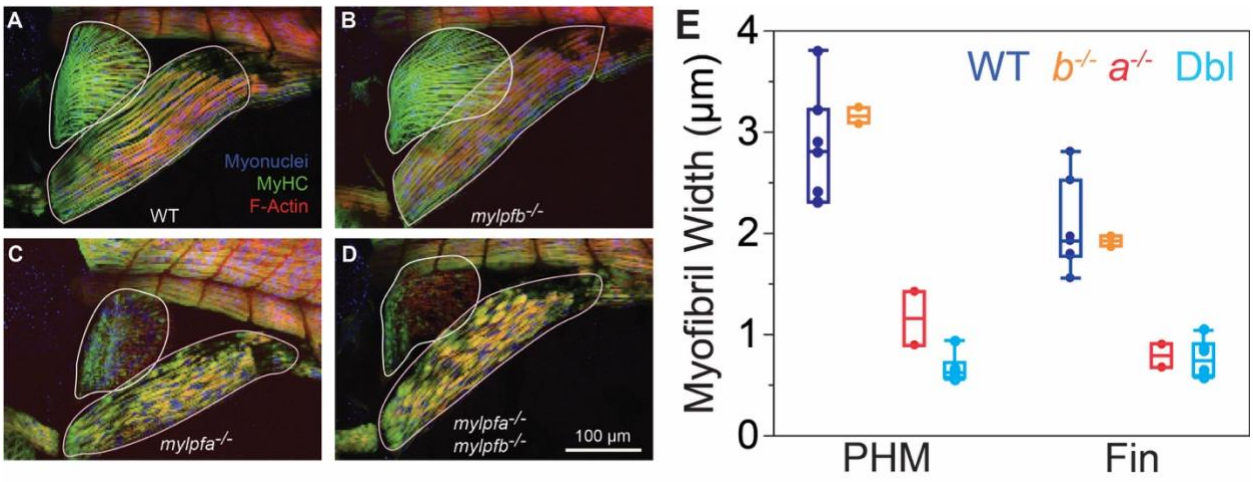

Figure 7. The Fin and PHM have severe muscle defects in the mylpfa$^{-/-}$ mutant and the mylpfa$^{-/-}$;mylpfb$^{-/-}$ double mutant. **(A-D)** Immunolabel of sarcomere components and myonuclei in WT (A), *mylpfb*$^{-/-}$ (B), *mylpfa*$^{-/-}$ (C), and the *mylpfa*$^{-/-}$*;mylpfb*$^{-/-}$ double mutant (D) shown via 3D renderings of the fin and PHM in a 3 dpf embryo. Phalloidin label marks F-actin (red), antibody A4.1025 (green) marks skeletal muscle MyHC and antibody to Rbfox1l marks myonuclei (blue). PHM and fin width demonstrate myofibrillar defects in the *mylpfa*$^{-/-}$ mutant and no myofibrils in the *mylpfa*$^{-/-}$*;mylpfb*$^{-/-}$ double mutant in both the PHM and fin fast-twitch muscle. The scale bar is 100 µm, applicable to A-D.

4.2. Mylpf Loss of Function Causes Impaired Pectoral Fin Cartilage Formation

Using a specific skeleton/ cartilage staining technique, Alcian/Alizarin Double stain, we found that the endochondral plate, analogous to the human distal limb, was explicitly reduced in the 6 dpf *mylpfa*^{oz30} zebrafish fin (Figure 8 A-C). Other cartilage elements, such as the scapulocoracoid, were often deformed but showed no reduction in cartilage area (quantification not shown). The endochondral plate in the 7 dpf mylpfa^{oz30} zebrafish fin showed no improvement in the cartilage area, indicating that the endochondral plate does not grow in mylpfa^{oz30} mutants between 6 dpf and 7 dpf (Figure 8 D-F). Initial analysis used our standard allele, *mylpfa*^{oz30}*,* and we confirmed the finding using a second frameshifting allele, mylpfa^{oz43}, also at 6 dpf, demonstrating that the reduction in endochondral plate area is not allele specific (Figure 8 G-I).

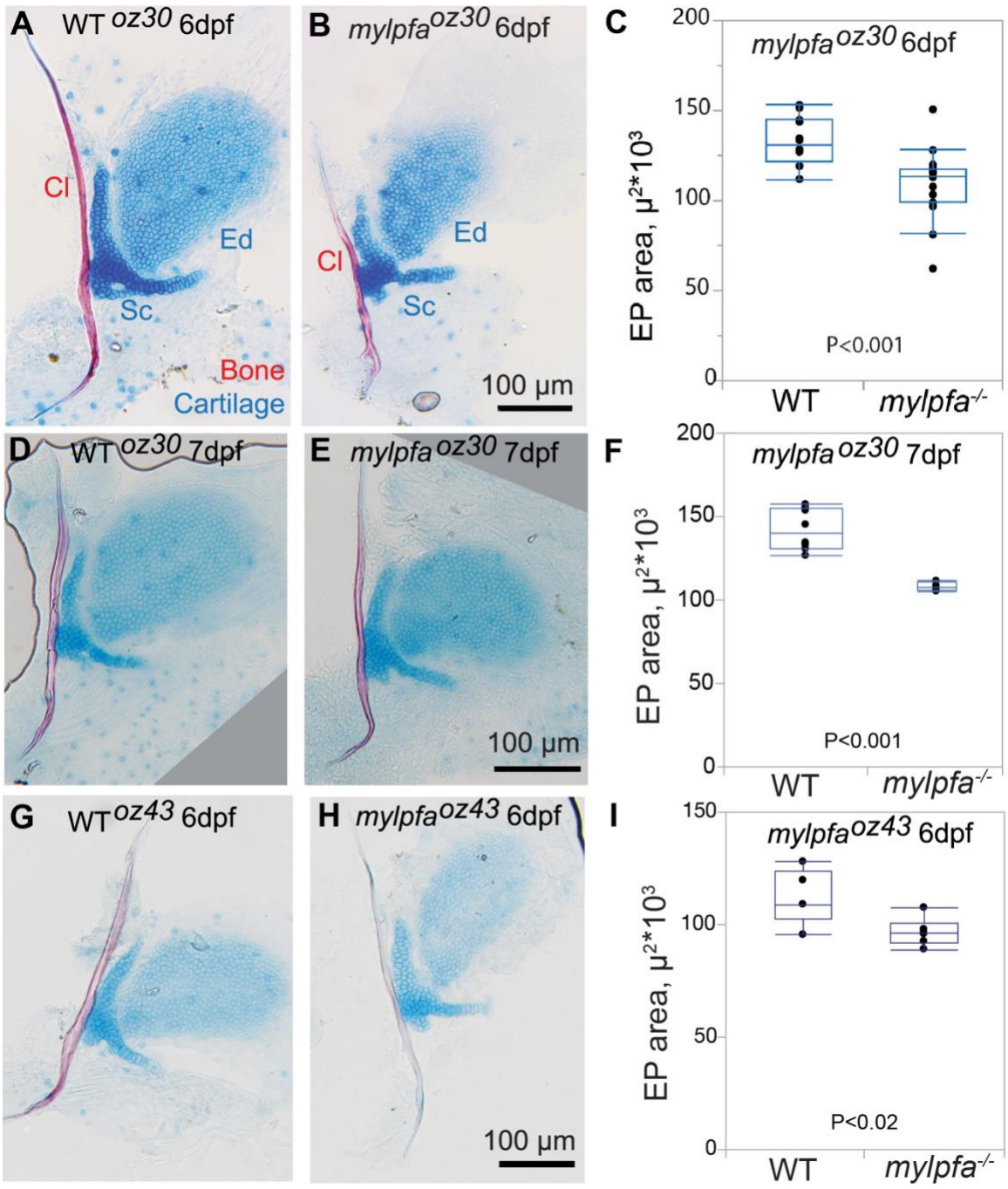

Figure 8. Endochondral plate area is significantly reduced in both *mylpfa* mutants. **(A-B, D-E, G-H)** Alcian/Alizarin Skeletal-Cartilage Stain for analysis of fin cartilage components in 6 dpf mylpfa^{oz30} embryos, 7 dpf mylpfa^{oz30} embryos, and in 6 dpf mylpfa^{oz43} embryos, respectively. **(C, F, I)** The mean endochondral plate area in multiple mylpfa alleles significantly re compared to WT. Scale bars in A-B, D-E, and G-H are 100 µm.

The 6 dpf WT and *mylpfb*$^{-/-}$ mutants have no significant difference in endochondral plate area (Figure 9 A-B, E). However, the 6dpf *mylpfa*$^{-/-}$ and *mylpfa*$^{-/-}$*;mylpfb*$^{-/-}$ double mutant endochondral plates both showed a significant reduction in endochondral plate area when compared to WT and *mylpfb*$^{-/-}$ mutants, mirroring myofibril width data in the fin and PHM (Figure 9 C-E). The *mylpfa*$^{-/-}$ and *mylpfa*$^{-/-}$*;mylpfb*$^{-/-}$ double mutant endochondral plate areas were not significantly different. This suggests that the pectoral fin paralysis found the *mylpfa*$^{-/-}$ mutant and that this paralysis is enough to result in cartilage deformities, so further Mylpf loss does not result in increased severity of cartilage deformities.

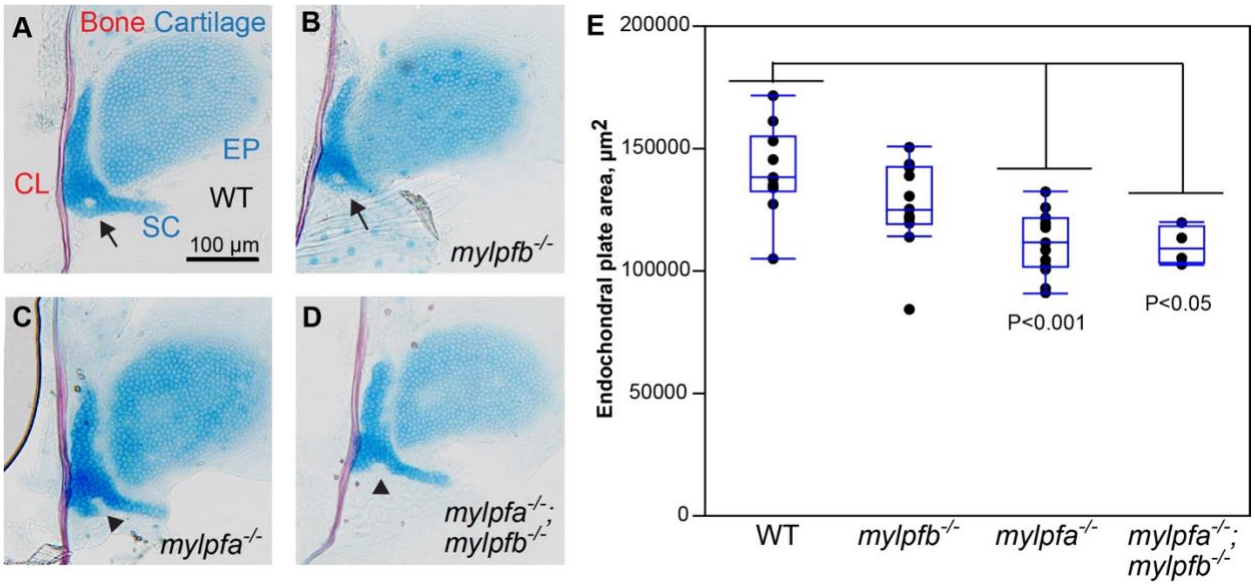

Figure 9. Endochondral plate area is reduced in Mylpf Mutants. **A-D.** Alcian/Alizarin Skeletal-Cartilage Stain for analysis of fin cartilage components. The endochondral plate area in WT is greater than *mylpfa*$^{-/-}$ and *mylpfa*$^{-/-}$*;mylpfb*$^{-/-}$ double mutants. **E.** *mylpfa*$^{-/-}$ ($p<0.001$) and *mylpfa*$^{-/-}$*;mylpfb*$^{-/-}$ double mutants ($p<0.05$) endochondral plate area is reduced when compared to WT and *mylpfb*$^{-/-}$ mutants. Scale bars in A-D are 100 µm. Significance thresholds were determined by Tukey-Kramer comparisons after one-way ANOVA.

We inferred that the reduction in cartilage formation may be due to impaired fin movement. To confirm this idea in a fully independent genetic context, we investigated cartilage development in *Δsix1a;4a*$^{-/-}$*;Δsix1b;4b*$^{-/-}$ mutant fish. The mutated genes (*six1a*, *six1b*, *six4a*, *six4b*) are required for muscle precursor movement away from somites and differentiation in the fin bud (Talbot et al., 2019). The *Δsix1a;4a*$^{-/-}$*;Δsix1b;4b*$^{-/-}$ genotype lacks all muscle in the fin, resulting in complete pectoral fin paralysis. Consistent with the *mylpfa*$^{-/-}$ mutant, preliminary analysis of *Δsix1a;4a*$^{-/-}$*;Δsix1b;4b*$^{-/-}$ mutant fish shows a pronounced reduction in the endochondral plate area, confirming impaired cartilage growth due to the loss of muscular contraction (Figure 10 A-C). These mutants also have defects not seen in the *mylpfa*$^{-/-}$ mutant, including a severe reduction in the scapulocoracoid area but not the cleithrum, suggesting that total muscle loss may have effects more severe than loss of muscle movement on the cartilage (Figure 10 D-E).

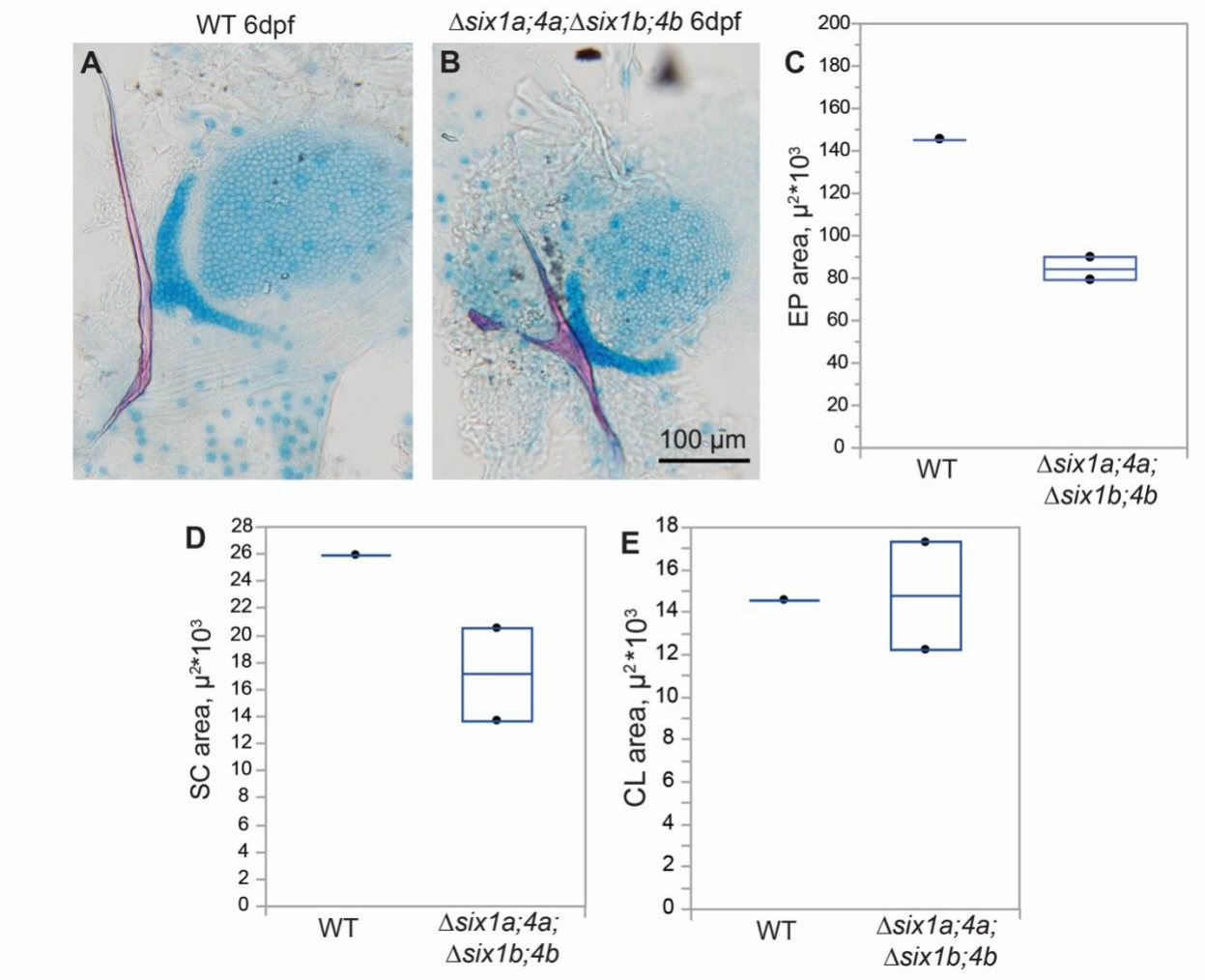

Figure 10. Endochondral plate and scapulocoracoid area is reduced in the *Δsix1a;4a*$^{-/-}$ *;Δsix1b;4b*$^{-/-}$ mutant. **A-B.** Alcian/Alizarin Skeletal-Cartilage Stain for analysis of fin cartilage components. **C-D.** Preliminary analysis suggests that the endochondral plate (C) and scapulocoracoid area (D) in WT is greater than *Δsix1a;4a*$^{-/-}$*;Δsix1b;4b*$^{-/-}$ mutant fish, who has no muscle fiber. **E.** The cleithrum is unchanged between genotypes. Scale bars in A-B are 100 µm.

4.3. A Model for Mylpf Function in Cartilage Development

We determined that mutations in the Mylpf gene impaired cartilage growth in the zebrafish pectoral fin, which is wholly composed of fast-twitch muscle. The endochondral plate area,

analogous to the human distal limb, was significantly reduced in multiple *mylpfa*$^{-/-}$ alleles at two developmental stages. Similarly, width analysis of the PHM and fin muscle and endochondral plate area demonstrated a significant reduction in width in both *mylpfa*$^{-/-}$ and *mylpfa*$^{-/-}$*;mylpfb*$^{-/-}$ double mutant when compared to WT and *mylpfb*$^{-/-}$ mutants. Both genotypes have severe muscle organization defects in the pectoral fins (Figure 7), and both show complete fin paralysis, so we infer that the paralysis experienced in the *mylpfa*$^{-/-}$ mutant is sufficient to cause cartilage deformities.

To independently confirm the effect of fin paralysis, we examined *Δsix1a;4a*$^{-/-}$*;Δsix1b;4b*$^{-/-}$ mutant fish, who lack all muscle hypaxial muscles, including the pectoral fin. These *Δsix1a;4a*$^{-/-}$*;Δsix1b;4b*$^{-/-}$ mutant fish, had a significant reduction in the endochondral plate area, further demonstrating impaired cartilage growth due to the loss of muscular contraction. During my time in the Talbot Lab, I was only about to analyze two *Δsix1a;4a*$^{-/-}$*;Δsix1b;4b*$^{-/-}$ mutant animals, so this work will need to be replicated before statistical analysis can be conducted. These results support that movement is key to stimulating proper cartilage development.

Our fin and PHM muscle analysis could also benefit from replicate studies. Although there are obvious differences in *mylpfa*$^{-/-}$ mutants and *mylpfa*$^{-/-}$*;mylpfb*$^{-/-}$ double mutants myofibrillar width, optimizing labeling and imaging procedures specific to the fin and PHM to achieve a higher sample size and sarcomericity analysis, as we accomplished in the trunk, may reveal more insights into how development varies in Mylpf mutants between the trunk and more

distal muscles. This could inform insights into why only certain cartilage elements of the pectoral fin are affected in Mylpf mutants.

Our interpretation of the Mylpf mutants and the *Δsix1a;4a*$^{-/-}$*;Δsix1b;4b*$^{-/-}$ mutant fish is predicated by the model that paralysis is the key feature leading to cartilage defects. We think that these genes are acting only indirectly on cartilage, in part because none of the mutant genes (*mylpfa*, *mylpfb*, *six1a, six4a*, *six1b*, *six4b*) are expressed in cartilage, and all are expressed in muscle (Jared C. Talbot et al., 2019). Furthermore, unpublished work by an undergraduate student in the Talbot Lab, Ryn Harrington, has explored the effect of paralysis directly. Ryn demonstrated a reduction in cartilage area when WT zebrafish were paralyzed at multiple stages with a muscle myosin inhibitor *N*-Benzyl-*p*-toluenesulfonamide (BTS). When BTS is applied beginning at 3 dpf when fin movement becomes apparent, the cartilage defects are very similar to what we found in the *mylpfa*$^{-/-}$ mutant. Earlier BTS treatments could produce even more severe fin cartilage defects, consistent with the observation that *Δsix1a;4a*$^{-/-}$*;Δsix1b;4b*$^{-/-}$ mutants have a more severe pectoral fin cartilage defect, suggesting that the presence of tensioned muscle may impact skeletal development even before movement begins. Our study, consistent with prior research in musculoskeletal development, indicates that paralysis or impaired movement results in skeletal abnormalities, such as those seen in arthrogryposis.

It has remained unclear whether DA is caused by muscle paralysis, muscle hypercontraction, or both. Our findings show that DA-like skeletal deformities can be induced by a loss of muscle function, either via muscle loss (*Δsix1a;4a*$^{-/-}$*;Δsix1b;4b*$^{-/-}$*),* myofibril loss (*mylpfa*$^{-/-}$ *and mylpfa*$^{-/-}$

;mylpfb$^{-/-}$) or straightforward paralysis (BTS). Our findings are consistent with standard models for DA onset in humans (J. G. Hall, 2014). However, prior studies investigating musculoskeletal formation in DA-causing gene variants in *Drosophila* suggested an overall shortening of the sarcomeres due to an enhanced contracted state of the myofibers; presumably, this shortening is related to the formation of contractures in DA patients (Whittle et al., 2021). Likewise, recent work with zebrafish bearing a DA mutation in the homologous residue of the gene Smyhc1 have slow-muscle hypercontraction, which can be rescued by muscle paralysis (Whittle et al., 2021). It remains possible that both modes of muscle disorder (hypercontraction and paralysis) can lead to matching skeletal deformities (Whittle et al., 2021), and future studies on human MYLPF variants may be key to understanding these gain and loss of function effects.

Research in chick embryos has demonstrated that movement post-paralysis can partially recover specific aspects of joint development, and the Talbot Lab's preliminary suggests that movement influences skeletal development in the pectoral fin before the active contractile muscle is present, providing possible insights and next steps with Mylpf zebrafish mutants (Harrington, 2023- Undergraduate Capstone; Rolfe et al., 2021). Future research focused on recovering Mylpf mutant cartilage deformities by manual movement could inform potential clinical treatments for DA1 patients.

Tension maintained by proper muscle development has long been implicated in skeletal development, especially in the joints (Hamburger & Waugh, 1940; Kahn et al., 2009; Murray & Drachman, 1969). A study of embryonic chick limbs demonstrates that cartilage is particularly sensitive to paralysis and experiences significant reductions in cartilage volumes compared to

skeletal elements (Osborne et al., 2002). Our findings suggest that the lack of muscular contraction, due to the failure of sarcomeres to form properly, results in reduced muscular tension needed to promote proper skeletal development. The reduction of tension due to the lack of sarcomeres forming complete myofibrils results in cartilage deformities, such as those seen in DA1.

In summary, we sought to investigate whether the flaccidity caused by Mylpf mutation could lead to a skeletal disorder that parallels limb contractures in DA1. Consistent with the model that DA1 arises by limb paralysis and the observations that fins are entirely paralyzed and lack fully functioning sarcomeres in the *mylpfa*$^{-/-}$ mutant, we determined the *mylpfa*$^{-/-}$ and the *mylpfa*$^{-/-}$*;mylpfb*$^{-/-}$ double mutant demonstrated a significant reduction in PHM and fin myofibril width and endochondral plate area. These results support that Mylpf gene function is needed for normal cartilage development in the zebrafish pectoral fin by promoting functional fast-twitch muscle fiber development.

CHAPTER 5

SUMMARY OF FINDINGS AND INTERPRETATION

Distal Arthrogryposis Type 1 (DA1) involves mild muscle weakness and limb skeletal abnormalities thought to be caused by paralysis in utero MYLPF variants have been established to underlie forms of DA1 in humans (Chong et al., 2020). Our findings support zebrafish Mylpf mutants as a DA model because these mutations cause both muscular and skeletal defects in the zebrafish pectoral fin. This study, to our knowledge, is the first ever study to examine both aspects of DA in a zebrafish genetic model. This study's findings suggest that Mylpf gene function is required for sarcomeric protein organization to promote normal fast-twitch muscle and cartilage development and that mutations in Mylpf result in cartilage deformities like those seen in DA1. In Mylpf mutants, we have demonstrated that there is partial sarcomere organization and myofibril development in the *mylpfa*$^{-/-}$ mutant with sarcomeres and myofibrils consistently absent in *mylpfa*$^{-/-}$*;mylpfb*$^{-/-}$ double mutant, suggesting that Mylpf is required for sarcomeric protein organization for normal fast-twitch muscle development. Similarly, width analysis of the PHM and fin muscle and endochondral plate area demonstrated a significant reduction in both *mylpfa*$^{-/-}$ and *mylpfa*$^{-/-}$*;mylpfb*$^{-/-}$ double mutant when compared to WT and *mylpfb*$^{-/-}$ mutants, supporting that Mylpf gene function is needed for normal cartilage development in the zebrafish pectoral fin by promoting functional fast-twitch muscle fiber development.

In summary, we have indicated through high-resolution image analysis that Mylpf gene function is required to promote functional fast-twitch muscle fiber development, which is needed for normal cartilage development in the zebrafish pectoral fin and is supported by the well-established model that movement and muscular tension is required for proper skeletal development. Our results build upon previous studies of Mylpf gene function in the etiology of DA1 in humans by revealing insights into Mylpf's role in fast-twitch muscle fiber development and how mutations in this gene can affect skeletal development.

CHAPTER 6

METHODS

6.1. Zebrafish Husbandry

Zebrafish were raised under standard conditions and staged as previously described in literature (Kimmel et al., 1995; Westerfield, 2007). Mutant lines utilized throughout this study are as follows: *mylpfa*^{oz30} (Chong et al., 2020), *mylpfa*^{oz43}(Chong et al., 2020),*mylpfb*^{oz39} (Unpublished), *Δsix1a;4a*^{oz27}(Talbot et al., 2019), and *Δsix1b;4b*^{oz16}(Talbot et al., 2019). The unpublished *mylpfb*^{oz39} line was developed by Dr. Talbot, Sarah Shepherd, and Emily Teets at The Ohio State University.

6.2. Immunohistochemistry

Immunohistochemistry is a technique used to identify specific proteins or antigens in tissues. It involves using antibodies that bind to the target protein or antigen and then detecting the bound antibodies using various methods, such as staining or fluorescence (Im, Mareninov, Diaz, & Yong, 2019). It allows for the visualization and localization of proteins within tissues. The protocols used in the Talbot Lab are similar to those previously established in the literature, though carefully optimized for our goals (Bird, Windner, & Devoto, 2012). Specific conditions follow. Immunolabel used the following antibodies: Rbfox1l (1:500) (Gallagher et al., 2011), A4.1025 (1:30, DSHB), and Phalloidin-568 (1:50, Invitrogen). A4.1025 was deposited to the DSHB by Blau, H.M. (DSHB Hybridoma Product A4.1025). The Rbfox1l and Phalloidin working

concentrations were established prior to my study; A4.1025 concentrations were re-optimized by Jared Austin as part of a capstone project in the Talbot lab. Immunolabel uses an established technique, with light modifications summarized as follows (Bird et al., 2012). Embryos were fixed in 4% PFA for two hours at room temperature, then washed out of fix using 1X Phosphate Buffered Saline Tween-20 (PBST) three times to ensure complete washing. Ten μg/mL ProteaseK (ProK) was added to the embryos for 40 minutes to permeabilize them for the antibodies. PBST was again used five times for complete washing, then placed in K block (1X PBS, 0.5% TritonX-100, 4% NGS, 2% NSS, 1% DMSO) for four to six hours at room temperature. 500 μL of the primary antibody solution was added to the embryos and allowed to rock overnight at four ˚C. The next day, embryos were washed out of the primary antibodies using PBST six to eight times over one to two hours. Secondary antibodies were added and rocked at room temperature for four hours. Secondary antibodies are Goat anti-Rabbit-488 (conc. 1:800) and Goat anti-Mouse IgG2a-647 (conc. 1:800); Phalloidin-546 was added two hours into this step. At this step, all embryos were kept covered to minimize photobleaching. Embryos were washed multiple times in PBST over an hour before being stored at four ˚C to await confocal imaging. Antibodies Goat-anti-Mouse IgG-647, Goat-anti-M IgG2b-488, anti-Actinin, anti-Titin (T9030), and Phalloidin-546 were utilized to examine sarcomere growth and development in Wild-Type fish at 24hpf, 48hpf, and 72hpf. 1 ml of 10 μg/ml ProK was added for 40 minutes to permeabilize the 48hpf and 72hpf embryos. All other immunolabeling steps are the same as listed above.

6.3. Alcian/Alizarin Double Stain

Zebrafish embryos were raised to either 6dpf or 7dpf and were given a lethal dose of tricaine for euthanasia**.** To prep them for Cartilage/ Skeleton Stain, as previously described, embryos were fixed in 2% PFA / 1X PBS for 1 hour (J. C. Talbot, Johnson, & Kimmel, 2010; Walker & Kimmel, 2007). Embryos were washed out of fix with 50% ethanol (EtOH), then placed in a solution of Double Stain (0.5% Alizarin Red and 0.2% Alcian Blue) overnight. This stain was washed in 80% EtOH/10mM MgCl2 for 30 mins, then in 50% and 25% Ethanol for 5 minutes each. Fresh mixed / with 0.5% KOH was added to the embryos, with tube caps open to prevent pressure buildup. Embryos were then rinsed two times in 25% glycerol/0.1% KOH for 10 minutes before being replaced with 50% glycerol/0.1% KOH and nutated for at least a few hours. The 50% glycerol/0.1% KOH was replaced, and stained embryos were stored at 4˚C to reduce fading. Alcian/Alizarin stained fish fins were dissected and then flat-mounted for imaging. Flat-mounted fins were then imaged on a dissecting scope to allow the cartilage and skeletal elements to be analyzed. ImageJ's polygon area selection tool was utilized to measure the area of specified cartilage elements. Two area measurements were taken per cartilage element and averaged per fish fin.

6.4. Genotyping

After fixing the embryos as appropriate per the experiment, the tails of each embryo were dissected, and both the trunk and tail regions were transferred to a labeled 96-well plate, respectively. Therompol Buffer solution with the ProteaseK (ProK) enzyme to break down the

tail sample for further analysis. Polymerase chain reaction (PCR) was then utilized to amplify our targeted DNA sequence using specific primers. Sometimes an additional digestion step was needed to analyze a sequence effectively. Genotyping procedures for *mylpfa* (Chong et al., 2020) and *Δsix1a;4a*$^{-/-}$*;Δsix1b;4b*$^{-/-}$ (Talbot et al., 2019) were as previously described in literature. Routine genotyping for *mylpfb*^{oz39} uses primers F 5'-GCAACAATGGGTCAGCTAATG-3' and R 5'-CCCAAAACCAAAAGTATGAG-3', then BccI digestion to cut the wildtype amplicon into two products (120 bp and 76 bp) while mutant amplicon (191 bp) remains uncut.

After PCR, gel electrophoresis determines each embryo's genotype by separating DNA based on size and charge. A gel is prepared by mixing a solution of 3% agarose with a buffer solution and Gel Red and allowed to solidify. Next, the PCR sample is mixed with a loading dye and loaded into wells on the gel. An electric current is then applied to the gel, causing the molecules to move through the gel matrix toward the opposite end of the gel. Smaller molecules move faster through the gel and travel further than larger molecules. As the molecules move through the gel, they separate into distinct bands, which can be visualized thanks to the addition of Gel Red through an image to identify the genotype per well.

6.5. Confocal Imaging

Confocal imaging allows us to capture high-resolution images of molecular substructures. It uses a laser to excite a specific region of the sample that has been fluorescently labeled, emitting fluorescent light captured by a detector. The laser is scanned across the sample in a series of thin slices, allowing for the creation of detailed 3D images. Embryos are mounted on a

slide on their sagittal plane using clear agarose. Dr. Talbot and I spent many days optimizing imaging conditions that give clear sub-sarcomere resolution on a Leica Sp8 confocal. We determined that a 25x water immersion lens with 3X line averaging and low speed (about a 30-minutes) was optimal for our imaging and subsequent image analysis. A few images were taken with a 63x Type-F oil immersion lens, but gathering these images was hindered by a poor working distance, resulting in slow imaging and exclusion of several samples that could not be reached with the lens. The ensuing 63x images have improved resolution but did not yield insights beyond what we show for those collected using the 25x water lens, so that slightly lower resolution technique has become our standard.

6.6. Sarcomericity Image Analysis Package

Various collaborators with the Talbot Lab developed a new technique to determine the degree of sarcomere organization deemed, Sarcomericity. This package was developed with additions from me, Dr. Joshua Kelley, Dr. Joy-El Talbot, and Dr. Jared Talbot to create a robust image analysis package to determine sarcomericity. It has been determined through confocal imaging sets ranging in magnification levels from 25x to 63x magnification that this method requires a certain image granularity (10-23 pixels/ μm) to be effective. At higher magnifications, the smaller pieces of a sarcomere (e.g., thick and thin filaments) dominate periodicity, and the periodicity disintegrates entirely.

To quantify sarcomericity, this method uses multiple Range of Interest (ROI) delineations in ImageJ to calculate intensity per ROI for each image channel. Then, peak-to-peak distances per

intensity are determined per image, then averaged to show bootstrap confidence intervals (CI) shown via histogram to represent the Fraction of Peaks/micron (μm). The histogram analysis is then used to determine Sarcomericity in MATLAB. The sarcomericity score is achieved by identifying the typical sarcomeric region in bin ranges for each marker, then by comparing the sum of the sarcomeric histogram region to the total. We have also included normalized grayscale values and mean sarcomeric and non-sarcomeric region calculations in the final exported CSV to provide a robust, unbiased image analysis tool.

6.6.1. ImageJ Macro Plugin- Sarcomere Quantification

Dr. Joy-el Talbot developed an ImageJ Macro plugin to analyze large datasets and easily export ROI multi-plot data over multiple channels. After folder selection and setting the scale for ROI selections, three subfolders are created via the macro to organize processed images, CSV data files, and ROI zip data. The user is then prompted to check the scaling by drawing an ROI over the scalebar on the image. Then, 30 ROI selections per image are suggested for accurate accrual of sarcomere organization data. Multi-plot data showing ROI intensity quantification per image channel (three total: Red, Green, and Blue) are exported via CSV file for further analysis.

6.6.2. MATLAB- Frequency by Peak for Sarcomericity Analysis

The exported CSV data using the Sarcomere Quantification ImageJ macro plugin are imported to MATLAB for further analysis. After data import, MATLAB first calculates the size of each ROI in pixels to then be calculated to microns. Then, a smoothing function is applied to reduce the noise in the dataset. After the noise reduction, MATLAB can determine all the maximum values,

or peaks, and distances between those maximum values within the combined data, analogous to sarcomere length. An automatic binning algorithm returns bins with a uniform width, chosen to cover the range of the distances between the maximum values and reveal the underlying shape of the distribution. This data is then normalized to the length of the ROI and the number of ROIs drawn per image. This normalized data is plotted on a histogram showing the overall sarcomere organization of an image by displaying the distance between peaks (sarcomere components) per micron versus the Fraction of Peaks/micron (μm) (sarcomere organization). The ROIs are also utilized to determine the mean grayscale value of the selected regions, which can be utilized to assess protein abundance. A sarcomeric bin region based on established sarcomere length data and optimization by the Talbot Lab is applied per immunolabel marker. This data is used to determine the sarcomeric and non-sarcomeric regions of each histogram per image. The sum of the sarcomeric region histogram area is then divided by the sum of the total histogram area to give our final value of Sarcomericity to represent the overall sarcomere organization per image on a logical zero-to-one scale. Mean Sarcomeric and Non-sarcomeric regions, Sarcomericity, and Mean Gray-Values per image are exported in one easy-to-analyze CSV file.

6.6.2.1. MATLAB- Combine with CI

After using the Frequency by Peak for Sarcomericity Analysis MATLAB Code, MATLAB files storing important data are sorted by genotype into separate folders. In this code, the peak-to-peak distances are averaged to show bootstrap confidence intervals via histogram to represent the Fraction of Peaks/micron (μm).

6.6.2.2. MATLAB- Sum Peaks with CI

All MATLAB files storing the combined CI data are then sorted into a separate folder for combination into a histogram plot, with a gray box to identify the sarcomeric area. The user is prompted to edit the plot colors and legend to represent each genotype.

6.7. Sarcomere Manual Measurement Image Analysis Package

An ImageJ macro plugin was developed to analyze large datasets and easily export length data. This allows for quick and efficient measurements of metrics such as sarcomere length and myofibril width. 30 ROI selections per image are suggested to allow for accurate averaging of length data, with all ROIs per image exported for analysis. All steps of the macro plugin are the same as the Sarcomere Quantification macro, except for the data type collected and exported. A simple MATLAB code averages ROI data per image and exports a combined CSV File containing averages of all images in a folder.

BIBLIOGRAPHY

Aoki, H., Sadoshima, J., & Izumo, S. (2000). Myosin light chain kinase mediates sarcomere organization during cardiac hypertrophy in vitro. *Nature Medicine*, *6*(2), 183–188. doi: 10.1038/72287

Bamshad, M., Van Heest, A. E., & Pleasure, D. (2009). Arthrogryposis: A Review and Update. *The Journal of Bone and Joint Surgery. American Volume.*, *91*(Suppl 4), 40–46. doi: 10.2106/JBJS.I.00281

Bird, N. C., Windner, S. E., & Devoto, S. H. (2012). Immunocytochemistry to Study Myogenesis in Zebrafish. In J. X. DiMario (Ed.), *Myogenesis* (pp. 153–169). Totowa, NJ: Humana Press. doi: 10.1007/978-1-61779-343-1_9

Bray, M.-A., Sheehy, S. P., & Parker, K. K. (2008). Sarcomere alignment is regulated by myocyte shape. *Cell Motility and the Cytoskeleton*, *65*(8), 641–651. doi: 10.1002/cm.20290

Busse, B., Galloway, J. L., Gray, R. S., Harris, M. P., & Kwon, R. Y. (2020). Zebrafish: An Emerging Model for Orthopedic Research. *Journal of Orthopaedic Research*, *38*(5), 925–936. doi: 10.1002/jor.24539

Cerna, M., & Harvey, A. F. (2000). The Fundamentals of FFT-Based Signal Analysis and Measurement. *National Instruments*. Retrieved from https://www.lumerink.com/courses/ECE697A/docs/Papers/The%20Fundamentals%20of%20FFT-Based%20Signal%20Analysis%20and%20Measurements.pdf

Chen, Z., Huang, W., Dahme, T., Rottbauer, W., Ackerman, M. J., & Xu, X. (2008). Depletion of zebrafish essential and regulatory myosin light chains reduces cardiac function through distinct mechanisms. *Cardiovascular Research*, *79*(1), 97–108. doi: 10.1093/cvr/cvn073

Chong, J. X., Talbot, J. C., Teets, E. M., Previs, S., Martin, B. L., Shively, K. M., … Bamshad, M. J. (2020). Mutations in MYLPF Cause a Novel Segmental Amyoplasia that Manifests as Distal Arthrogryposis. *The American Journal of Human Genetics*, *107*(2), 293–310. doi: 10.1016/j.ajhg.2020.06.014

Clack, J. A. (2009). The Fin to Limb Transition: New Data, Interpretations, and Hypotheses from Paleontology and Developmental Biology. *Annual Review of Earth and Planetary Sciences*, *37*(1), 163–179. doi: 10.1146/annurev.earth.36.031207.124146

Coates, M. I., Ruta, M., & Friedman, M. (2008). Ever Since Owen: Changing Perspectives on the Early Evolution of Tetrapods. *Annual Review of Ecology, Evolution, and Systematics*, *39*(1), 571–592. doi: 10.1146/annurev.ecolsys.38.091206.095546

Diogo, R., Ziermann, J. M., Molnar, J., Siomava, N., & Abdala, V. (2018). *Muscles of chordates: Development, homologies, and evolution*. Boca Raton: CRC Press, Taylor & Francis Group.

Dunn, K. W., Kamocka, M. M., & McDonald, J. H. (2011). A practical guide to evaluating colocalization in biological microscopy. *American Journal of Physiology-Cell Physiology*, *300*(4), C723–C742. doi: 10.1152/ajpcell.00462.2010

Gallagher, T. L., Arribere, J. A., Geurts, P. A., Exner, C. R. T., McDonald, K. L., Dill, K. K., … Conboy, J. G. (2011). Rbfox-regulated alternative splicing is critical for zebrafish cardiac and skeletal muscle function. *Developmental Biology*, *359*(2), 251–261. doi: 10.1016/j.ydbio.2011.08.025

Gehrke, A. R., Schneider, I., de la Calle-Mustienes, E., Tena, J. J., Gomez-Marin, C., Chandran, M., … Shubin, N. H. (2015). Deep conservation of wrist and digit enhancers in fish. *Proceedings of the National Academy of Sciences*, *112*(3), 803–808. doi: 10.1073/pnas.1420208112

Grandel, H., & Schulte-Merker, S. (1998). The development of the paired fins in the zebrafish (Danio rerio). *Mechanisms of Development*, *79*(1–2), 99–120. doi: 10.1016/s0925-4773(98)00176-2

Hall, B. K., & Herring, S. W. (1990). Paralysis and growth of the musculoskeletal system in the embryonic chick. *Journal of Morphology*, *206*(1), 45–56. doi: 10.1002/jmor.1052060105

Hall, J. G. (2014). Arthrogryposis (multiple congenital contractures): Diagnostic approach to etiology, classification, genetics, and general principles. *European Journal of Medical Genetics*, *57*(8), 464–472. doi: 10.1016/j.ejmg.2014.03.008

Hall, J. G., & Kiefer, J. (2016). Arthrogryposis as a Syndrome: Gene Ontology Analysis. *Molecular Syndromology*, *7*(3), 101–109. doi: 10.1159/000446617

Hamburger, V., & Waugh, M. (1940). The Primary Development of the Skeleton in Nerveless and Poorly Innervated Limb Transplants of Chick Embryos. *Physiological Zoology*, *13*(4), 367–382. doi: 10.1086/physzool.13.4.30151585

Harrington, R. (2023). *Muscle actvity promotes skeletal development in the zebrafish pectoral fin even before fins become mobile.* University of Maine.

Huxley, A. F. (2000). Cross-bridge action: Present views, prospects, and unknowns. *Journal of Biomechanics*, *33*(10), 1189–1195. doi: 10.1016/S0021-9290(00)00060-9

Im, K., Mareninov, S., Diaz, M. F. P., & Yong, W. H. (2019). An Introduction to Performing Immunofluorescence Staining. In W. H. Yong (Ed.), *Biobanking* (pp. 299–311). New York, NY: Springer New York. doi: 10.1007/978-1-4939-8935-5_26

Kahn, J., Shwartz, Y., Blitz, E., Krief, S., Sharir, A., Breitel, Dario. A., … Zelzer, E. (2009). Muscle Contraction Is Necessary to Maintain Joint Progenitor Cell Fate. *Developmental Cell*, *16*(5), 734–743. doi: 10.1016/j.devcel.2009.04.013

Kilroy, E. A., Ignacz, A. C., Brann, K. L., Schaffer, C. E., Varney, D., Alrowaished, S. S., … Henry, C. A. (2022). Beneficial impacts of neuromuscular electrical stimulation on muscle structure and function in the zebrafish model of Duchenne muscular dystrophy. *ELife*, *11*, e62760. doi: 10.7554/eLife.62760

Kimmel, C. B., Ballard, W. W., Kimmel, S. R., Ullmann, B., & Schilling, T. F. (1995). Stages of embryonic development of the zebrafish. *Developmental Dynamics*, *203*(3), 253–310. doi: 10.1002/aja.1002030302

Kimmel, C. B., Wind, A. L., Oliva, W., Ahlquist, S. D., Walker, C., Dowd, J., … Nichols, J. T. (2021). Transgene-mediated skeletal phenotypic variation in zebrafish. *Journal of Fish Biology*, *98*(4), 956–970. doi: 10.1111/jfb.14300

Krans, Jacob L. (2010). The Sliding Filament Theory of Muscle Contraction. *Nature Education*, *3*(9), 66.

Lagache, T., Grassart, A., Dallongeville, S., Faklaris, O., Sauvonnet, N., Dufour, A., … Olivo-Marin, J.-C. (2018). Mapping molecular assemblies with fluorescence microscopy and object-based spatial statistics. *Nature Communications*, *9*(1), 698. doi: 10.1038/s41467-018-03053-x

Li, M., & Arner, A. (2015). Immobilization of Dystrophin and Laminin α2-Chain Deficient Zebrafish Larvae In Vivo Prevents the Development of Muscular Dystrophy. *PLOS ONE*, *10*(11), e0139483. doi: 10.1371/journal.pone.0139483

Lowey, S., & Trybus, K. M. (2010). Common Structural Motifs for the Regulation of Divergent Class II Myosins. *Journal of Biological Chemistry*, *285*(22), 16403–16407. doi: 10.1074/jbc.R109.025551

Luis, N. M., & Schnorrer, F. (2021). Mechanobiology of muscle and myofibril morphogenesis. *Cells & Development*, *168*, 203760. doi: 10.1016/j.cdev.2021.203760

Mao, Q., Acharya, A., Rodríguez-delaRosa, A., Marchiano, F., Dehapiot, B., Al Tanoury, Z., … Schnorrer, F. (2022). Tension-driven multi-scale self-organisation in human iPSC-derived muscle fibers. *ELife*, *11*, e76649. doi: 10.7554/eLife.76649

Mercader, N. (2007). Early steps of paired fin development in zebrafish compared with tetrapod limb development. *Development, Growth & Differentiation*, *49*(6), 421–437. doi: 10.1111/j.1440-169X.2007.00942.x

Murray, P. D., & Drachman, D. B. (1969). The role of movement in the development of joints and related structures: The head and neck in the chick embryo. *Journal of Embryology and Experimental Morphology*, *22*(3), 349–371.

Myachina, T. A., & Lookin, O. N. (2020). A Configurable Algorithm for Determining the Mean Sarcomere Length of a Cardiomyocyte By Discrete Fourier Transform. In S. Pinelas, A. Kim, & V. Vlasov (Eds.), *Mathematical Analysis With Applications* (pp. 265–272). Cham: Springer International Publishing. doi: 10.1007/978-3-030-42176-2_26

Nakamura, T., Gehrke, A. R., Lemberg, J., Szymaszek, J., & Shubin, N. H. (2016). Digits and fin rays share common developmental histories. *Nature*, *537*(7619), 225–228. doi: 10.1038/nature19322

Nakamura, T., Schneider, I., & Shubin, N. H. (2021). Evolution: The deep genetic roots of tetrapod-specific traits. *Current Biology*, *31*(10), R467–R469. doi: 10.1016/j.cub.2021.03.096

Osborne, A. C., Lamb, K. J., Lewthwaite, J. C., Dowthwaite, G. P., & Pitsillides, A. A. (2002). *Short-term rigid and flaccid paralyses diminish growth of embryonic chick limbs and abrogate joint cavity formation but differentially preserve pre-cavitated joints*.

Parsons, S., Boonman, A. M., & Obrist, M. K. (2000). Advantages and Disadvantages of Techniques for Transforming and Analyzing Chiropteran Echolocation Calls. *Journal of Mammalogy*, *81*(4), 927–938. doi: 10.1644/1545-1542(2000)081<0927:AADOTF>2.0.CO;2

Pasqualini, F. S., Sheehy, S. P., Agarwal, A., Aratyn-Schaus, Y., & Parker, K. K. (2015). Structural Phenotyping of Stem Cell-Derived Cardiomyocytes. *Stem Cell Reports*, *4*(3), 340–347. doi: 10.1016/j.stemcr.2015.01.020

Rolfe, R. A., Scanlon O'Callaghan, D., & Murphy, P. (2021). Joint development recovery on resumption of embryonic movement following paralysis. *Disease Models & Mechanisms*, *14*(4), dmm048913. doi: 10.1242/dmm.048913

Rui, Y., Bai, J., & Perrimon, N. (2010). Sarcomere Formation Occurs by the Assembly of Multiple Latent Protein Complexes. *PLoS Genetics*, *6*(11), e1001208. doi: 10.1371/journal.pgen.1001208

Salick, M. R., Napiwocki, B. N., Kruepke, R. A., Knight, G. T., Ashton, R. S., & Crone, W. C. (2020). The scanning gradient Fourier transform (SGFT) method for assessing sarcomere organization and alignment. *Journal of Applied Physics*, *127*(19), 194701. doi: 10.1063/1.5129347

Sanger, J. W., Wang, J., Fan, Y., White, J., & Sanger, J. M. (2010). Assembly and Dynamics of Myofibrils. *Journal of Biomedicine and Biotechnology*, *2010*, 1–8. doi: 10.1155/2010/858606

Schneider, I., & Shubin, N. H. (2013). The origin of the tetrapod limb: From expeditions to enhancers. *Trends in Genetics*, *29*(7), 419–426. doi: 10.1016/j.tig.2013.01.012

Sheth, R., Marcon, L., Félix Bastida, M., Junco, M., Quintana, L., Dahn, R., … Ros, M. A. (2012). Hox Genes Regulate Digit Patterning by Controlling the Wavelength of a Turing-Type Mechanism. *Science (New York, N.Y.)*, *338*(6113), 1476–1480. doi: 10.1126/science.1226804

Shwartz, Y., Farkas, Z., Stern, T., Aszódi, A., & Zelzer, E. (2012). Muscle contraction controls skeletal morphogenesis through regulation of chondrocyte convergent extension. *Developmental Biology*, *370*(1), 154–163. doi: 10.1016/j.ydbio.2012.07.026

Sitbon, Y. H., Yadav, S., Kazmierczak, K., & Cordary, D. S. (2020). Insights into myosin regulatory and essential light chains: A focus on their roles in cardiac and skeletal muscle function, development and disease. *Journal of Muscle Research and Cell Motility*, *41*(4), 313–327. doi: 10.1007/s10974-019-09517-x

Stein, J. M., Arslan, U., Franken, M., de Greef, J. C., E. Harding, S., Mohammadi, N., … van Meer, B. J. (2022). Software Tool for Automatic Quantification of Sarcomere Length and Organization in Fixed and Live 2D and 3D Muscle Cell Cultures *In Vitro*. *Current Protocols*, *2*(7). doi: 10.1002/cpz1.462

Sutcliffe, M. D., Tan, P. M., Fernandez-Perez, A., Nam, Y.-J., Munshi, N. V., & Saucerman, J. J. (2018). High content analysis identifies unique morphological features of reprogrammed cardiomyocytes. *Scientific Reports*, *8*(1), 1258. doi: 10.1038/s41598-018-19539-z

Talbot, J. C., Johnson, S. L., & Kimmel, C. B. (2010). Hand2 and Dlx genes specify dorsal, intermediate and ventral domains within zebrafish pharyngeal arches. *Development*, *137*(15), 2507–2517. doi: 10.1242/dev.049700

Talbot, Jared C., Teets, E. M., Ratnayake, D., Duy, P. Q., Currie, P. D., & Amacher, S. L. (2019). Muscle precursor cell movements in zebrafish are dynamic and require *six*- family genes. *Development*, dev.171421. doi: 10.1242/dev.171421

Teets, E. (2018). *The fast muscle Myosin light chain mylpfa is essential for fast muscle function and integrity*. The Ohio State University.

Tulenko, F. J., & Currie, P. D. (2021). Bones of contention: Skeletal patterning across the fin-to-limb transition. *Cell*, *184*(4), 854–856. doi: 10.1016/j.cell.2021.01.039

Walker, M., & Kimmel, C. (2007). A two-color acid-free cartilage and bone stain for zebrafish larvae. *Biotechnic & Histochemistry*, *82*(1), 23–28. doi: 10.1080/10520290701333558

Wang, Y., Szczesna-Cordary, D., Craig, R., Diaz-Perez, Z., Guzman, G., Miller, T., & Potter, J. D. (2007). Fast skeletal muscle regulatory light chain is required for fast and slow skeletal muscle development. *The FASEB Journal*, *21*(9), 2205–2214. doi: 10.1096/fj.06-7538com

Wang, Z., Grange, M., Wagner, T., Kho, A. L., Gautel, M., & Raunser, S. (2021). The molecular basis for sarcomere organization in vertebrate skeletal muscle. *Cell*, *184*(8), 2135-2150.e13. doi: 10.1016/j.cell.2021.02.047

Waterman, S. (2023). *Muscle-specific Disparities in Mylpf Sensitivity May Explain the Defining Symptoms of Distal Arthrogryposis*. The University of Maine.

Westerfield, M. (2007). *The Zebrafish Book. A Guide for the Laboratory Use of Zebrafish (Danio rerio)* (5th Edition). University of Oregon Press, Eugene.

Whittle, J., Johnson, A., Dobbs, M. B., & Gurnett, C. A. (2021). Models of Distal Arthrogryposis and Lethal Congenital Contracture Syndrome. *Genes*, *12*(6), 943. doi: 10.3390/genes12060943

Wood, T. W. P., & Nakamura, T. (2018). Problems in Fish-to-Tetrapod Transition: Genetic Expeditions Into Old Specimens. *Frontiers in Cell and Developmental Biology*, *6*, 70. doi: 10.3389/fcell.2018.00070

Xu, J., Gao, J., Li, J., Xue, L., Clark, K. J., Ekker, S. C., & Du, S. J. (2012). Functional Analysis of Slow Myosin Heavy Chain 1 and Myomesin-3 in Sarcomere Organization in Zebrafish Embryonic Slow Muscles. *Journal of Genetics and Genomics*, *39*(2), 69–80. doi: 10.1016/j.jgg.2012.01.005

AUTHOR BIOGRAPHY

Emily Tomak obtained a B.S. in Ecology and Environmental Science with a concentration in Natural History and Environmental Studies and a minor in Pre-Medical Studies from the University of Maine in May 2021. After her B.S., she expanded her scientific understanding by studying musculoskeletal disease development in the Talbot lab. Throughout her master's work, she taught in various capacities- as a biology lab Teaching assistant and rock climbing instructor. She plans to continue teaching as a high school life science teacher. She is a candidate for the Master of Science degree in Biological Sciences from the University of Maine in August 2023.